Contents lists available at ScienceDirect

Arabian Journal of Chemistry

journal homepage: www.ksu.edu.sa

Original article

Sodium dodecyl sulphate-treated nanohydroxyapatite as an efficient shale stabilizer for water-based drilling fluids

Jeffrey O. Oseh [a,b,c,d,*], M.N.A.M. Norddin [a,b,c,*], Issham Ismail [a,b], Ugochukwu I. Duru [d], Eugene N. Ngouangna [a,b], Afeez O. Gbadamosi [e], Augustine Agi [f], Muftahu N. Yahya [a,b,g], Abdirahim O. Abdillahi [a,b], Ifeanyi A. Oguamah [d], Shaziera B. Omar [a,b]

[a] Department of Petroleum Engineering, Faculty of Chemical and Energy Engineering, Universiti Teknologi Malaysia, 81310 Johor Bahru, Malaysia
[b] Malaysia Petroleum Resources Corporation Institute for Oil and Gas (MPRC–UTM), Universiti Teknologi Malaysia, 81310 Johor Bahru, Malaysia
[c] Advanced Membrane Technology Research Centre (AMTEC), Nanostructured Materials Research Group (NMRG) – MD – Frontier Materials, Universiti Teknologi Malaysia, 81310 Johor Bahru, Malaysia
[d] Department of Petroleum Engineering, School of Engineering and Engineering Technology, Federal University of Technology, P.M.B. 1526 Owerri, Imo State, Nigeria
[e] Department of Petroleum Engineering, King Fahd University of Petroleum and Minerals, Dhahran, 31261, Saudi Arabia
[f] Faculty of Chemical and Process Engineering Technology, College of Engineering Technology, Universiti Malaysia Pahang, 26300, Gambang, Pahang, Malaysia
[g] Department of Chemical and Petroleum Engineering, Bayero University, Gwarzo Road Kano, Kano, PMB 3011, Nigeria

ARTICLE INFO

Keywords:
Hot-rolling dispersion
Shale swelling
Nanohydroxyapatite
Sodium dodecyl sulphate
Water-based drilling mud
Suspension stability

ABSTRACT

Drilling water-sensitive shale formations often leads to wellbore instability, resulting in drilling problems because of the clay's high-water affinity. To solve this problem, different nanoparticles (NPs), such as nanosilica, have been used to formulate water-based muds with potassium chloride (KCl-WBM). Nevertheless, the unmatched pore size of shale pores when using nanosilica fails to completely prevent shale swelling and dispersion. This study discusses the effects of KCl-WBM with sodium dodecyl sulphate-treated nanohydroxyapatite (nHAp/SDS) on shale swelling inhibition through various laboratory techniques. These techniques encompass the linear swell meter (LSM), the dynamic linear swell meter (DLSM), hot-rolling dispersion, suspension stability, and pore structure characterization of shale. The rheological and filtration characteristics of nHAp/SDS and compatibility tests were also studied, and the results were compared with those of nanosilica and KCl-WBM. At all concentrations, the performance of the nHAp/SDS test fluids surpassed that of nanosilica. When compared with KCl-WBM system at 10 cP and 25 °C, the nHAp/SDS and nanosilica concentrations increased the plastic viscosity by 20–90 % and 10–70 %, respectively. The inhibitory effect of nHAp/SDS surpasses that of conventional KCl-WBM and inorganic nanosilica. By adding 2.0 wt% nHAp/SDS to KCl-WBM, the shale swelling decreased from 10.1 to 4.7 % (a 53.4 % reduction). Nanosilica also reduced the swelling to 6.1 % (a 39.6 % reduction) during the LSM test at 25 °C. Under the DLSM test conditions, the shale swelling increased due to the activation of the clay platelet site at an increased temperature of 80 °C. For instance, between 25 and 80 °C, the DLSM test revealed that the shale plug height expanded from 6.1 to 9.8 % for 2.0 wt% nanosilica, 4.7–7.6 % for 2.0 wt% nHAp/SDS, and 10.1–18.8 % for KCl-WBM. Furthermore, the recovery rate of hot-rolled shale plugs with KCl-WBM increased from 89.8 to 96.2 % for nHAp/SDS and 76.6 to 88.8 % for nanosilica from the initial rates of 52.1–63.3 % between 65 and 120 °C. The contact angle results showed that nHAp/SDS is hydrophobic, reducing shale-water attraction. Moreover, the 12 nm nanosilica matches nanopore sizes to partially block shale pores. This research found that nHAp/SDS has the potential to improve wellbore stability.

1. Introduction

Not long ago, the oil industry viewed shales as a drawback when drilling for limestone and sandstones rocks (Al-Bazali et al., 2021). Shales are rocks with low permeability characterized by narrow pore diameters and containing clay minerals, calcite, and quartz (Zhong et al., 2020). Shales make up 75 % of formations explored in oil and gas drilling and are responsible for 90 % of wellbore instability issues, such as well collapses, cavings, tight holes, and trapped pipes (Zhong et al.,

* Corresponding authors.
E-mail addresses: jeffreyoseh@utm.my (J.O. Oseh), anam@utm.my (M.N.A.M. Norddin).

https://doi.org/10.1016/j.arabjc.2024.105760
Received 29 January 2024; Accepted 24 March 2024
Available online 28 March 2024

2020). In recent decades, considerable effort has been dedicated to solving these challenging issues through the use of drilling mud. Field operations typically prioritize the use of water-based mud (WBM) systems due to the various issues linked to conventional oil-based muds (OBMs), like strict environmental regulations and higher operating costs, which hinder the deployment of OBM in drilling shale formations (Tian et al., 2021). Thus, the quest for eco-friendly WBMs that reduce fluid-shale contact and mimic OBM properties is a current focus of study (Huang et al., 2020).

Clay swelling during drilling poses a significant challenge for shale drilling operators due to the potential setbacks it can cause, such as extended drilling time and higher expenses (Saleh et al., 2021). The expansion of water-sensitive clays in shale deposits leads to shale falling into boreholes, which in turn causes string pack-off, a reduction in wellbore diameter, and drill pipe sticking (Hale and Mody, 1993). Particles rich in organic matter and mostly clay-sized, such as smectite clays, have high hydration levels and tend to expand, leading to drilling problems (Zhong et al., 2012). These drilling problems may have stemmed from the interaction between water and underground wellbore clay minerals, resulting in some unfavourable wellbore alterations. These factors encompass inadequate cleaning of the wellbore, well collapse, and a reduced drilling rate (ROP) due to overburden stresses and diagenesis (Zarei and Nasiri, 2021). These issues may also cause a significant increase in circulation density (ECD), leading to downtime (Zhong et al., 2012). This occurs due to shale dispersion and hydration, the development of microfractures on the shale surface, and a reduction in the formation's mechanical properties (Mao et al., 2015).

Most WBM inhibitors include potassium chloride (KCl) to prevent clay expansion, hydration, and borehole collapse (Sehly et al., 2015; Huang et al., 2020). Shale collapse, sloughing, and dispersion may occur from clay swelling and hydration, which must be considered while preparing drilling fluids (Al-Bazali et al., 2021; Huang et al., 2020). Numerous studies have examined KCl's capability of inhibiting clay water absorption and expansion. It is widely accepted that this inhibitory ability is dependent on the potassium ions (K^+) present in KCl (Al-Bazali et al., 2021; Huang et al., 2020; Sehly et al., 2015; Steiger, 1982). Low-hydration-energy K^+ ions move through the gaps between clay layers and stick to the surface with a small amount of KCl. This hinders shale from absorbing water (Huang et al., 2020). With a high KCl amount, K^+ ions repel shale edge-to-edge, expelling it from water. In other words, KCl lowers the swelling of shale, but too much of it can lead to drop-off, shrinking, borehole degradation, and harmful benthic organisms (Steiger, 1982).

Several advancements have been made to produce efficient shale inhibitors for better reservoir protection. Hydrolyzed polyacrylamide (HPAM) (Zaitoun and Berton, 1996; Hale and Mody, 1993), polyanionic cellulose (PAC) (Villada et al., 2017), xanthan gum (XGD) (Villada et al., 2017), ionic liquids (Moukoko et al., 2023; Rahman et al., 2021), ionic polymeric liquids (Yang et al., 2017), quaternary gelatin ammonium salt (Li et al., 2019) are some of these inhibitors. Some other types are polyether diamine (Zhong et al., 2012), alkyl polyamine (Xie et al., 2022), terminated amine (Bai et al., 2017), reactive non-ionic polyglycols (Ferreira et al., 2016), polyethylene-mine (An and Yu, 2018), and organosilicate inhibitive polymer for high temperature (Zhang et al., 2020). When dealing with high-temperature wells, it is important to consider that inorganic salts and amine derivatives may not be effective as clay swelling inhibitors due to their toxic nature and rapid degradation (Barati et al., 2017). Another effective option to prevent shale swelling is polymer latex, but its limited thermal stability and suspension retention make it unsuitable for use in oil and gas fields (Xu et al., 2017). Besides that, conventional shale inhibitors might either stick together too easily or are too big to plug nanopores and decrease shale-fluid interactions, which would not be ideal for wellbore stability (Abdullah et al., 2022). Hence, the introduction of nanoparticles (NPs) in the oil and gas sector was considered a promising solution to enhance wellbore stability.

Recent research indicates that incorporating NPs into WBM has helped to seal shale pores. This sealing process can vary based on factors such as NP size, concentration, shale formation, reactive-clay minerals, and drilling fluid components (Sudharsan and Khare, 2023; Abdullah et al., 2022). Colloidal inorganic nanosilica particles, either alone or with polymers, have been used to plug shale pores because they can fit precisely into the pores (Zarei and Nasiri, 2021; Mao et al., 2015). Nevertheless, because of their tendency to agglomerate, attraction to water, and lack of effectiveness in sealing microcracks, they are unable to completely eliminate borehole instability. NPs tend to aggregate and agglomerate because their high surface energy makes the particles strongly attract each other (Zarei and Nasiri, 2021). This has impacted

Nomenclature

10 s	Gel strength at 10 s
10 min GS	Gel strength at 10 min
API	American petroleum institute
API FL	API filtrate loss
AV	Apparent viscosity
$CaCO_3$	Calcium carbonate
DTG	Derivative Thermogravimetry
EDX	Energy dispersive X-ray
FCT	Filter cake thickness
FL	Fluid loss volume
FTIR	Fourier transform infrared spectroscopy
HAp	Hydroxyapatite
HCl	Hydrochloric acid
KCl	Potassium chloride
LSM	Linear swell meter
Na_2HPO_4	Disodium hydrogen phosphate
XGD	Xanthan gum
WBDF	Water-based drilling fluid
HPDF	High-performance drilling fluid
PAC-LV	Low viscosity-polyanionic cellulose
Nanosilica	Silica nanoparticle
NaOH	Caustic soda
nHAp	Nanohydroxyapatite
nHAp/SDS	SDS-treated nanohydroxyapatite
NPs	Nanoparticles
OBM	Oil-based mud
PAC-R	Polyanionic cellulose reagent
DLSM	Dynamic linear swell meter
HTHP	High-temperature high-pressure
PSD	Particle size distribution
PV	Plastic viscosity
SDS	Sodium dodecyl sulphate
SEM	Scanning electron microscope
TEM	Transmission electron microscopy
TGA	Thermogravimetric analysis
WBM	Water-based mud
XRD	X-ray diffraction
YP	Yield point
ZP	Zeta potential

the dispersion and distribution of NPs in suspensions with polymers or microparticles (Elochukwu et al., 2017). Thus, dispersed nanosized particles with a diameter that aligns with shale pores and cracks could enhance borehole stability (Zarei and Nasiri, 2021). Utilizing a nanosized material with specific functional groups and surface chemistry can enhance shale stability in WBM, as demonstrated in recent studies (Sudharsan and Kare, 2023; Abdullah et al., 2022).

Lately, the growing utilization of nanoscale materials like hydroxyapatite (HAp) has heightened the significance of nanotechnology in the bioceramics field. HAp is a natural mineral composed of calcium and phosphate, with a chemical formula of $Ca_{10}(PO_4)_6(OH)_2$. This represents the crystal unit cell of two distinct entities (Córdova-Udaeta et al., 2021; Manafi et al., 2008). The main components of HAp are calcium and phosphate in a ratio of 1.67:1 (1.664 ± 0.005) (Prasad et al., 2023; Bulina et al., 2021). This substance is bioactive, non-hazardous, and cost-effective to manufacture (Prasad et al., 2023). Moreover, it contains a variety of functional groups (OH^-, PO_4^{3-}, and CO_3^{2-}) that facilitate simple surface modification (Koroleva et al., 2020). HAp demonstrates exceptional thermal stability, withstanding temperatures exceeding 600 °C without any degradation (Ngouangna et al., 2022a; Bulina et al., 2021). Furthermore, the effectiveness of HAp, similar to other NPs, relies on its surface characteristics, which can be enhanced through surfactant modification (Prakash et al., 2021). An improved form of HAp can result in a diameter size within the nanometer range, known as nanohydroxyapatite (nHAp).

Sodium dodecyl sulphate (SDS) has been identified as a highly effective particle modifier in recent studies (Qiao et al., 2016; Li and Ishiguro, 2016; Prasad et al., 2023). The authors utilized SDS to synthesize nHAp (referred to as nHAp/SDS), which has demonstrated enhancements in surface characteristics, particle dispersion, colloidal fluid stability, and interactions with drilling fluids. This indicates its potential for enhancing wellbore stability (Ngouangna et al., 2022b; Oseh et al., 2023a). Recently, the nHAp/SDS combination has enhanced the capacity of drilling fluid by reducing fluid loss and improving rheology. Water-based bentonite solutions were less impacted by salt when nHAp/SDS was used (Oseh et al., 2023a; Oseh et al., 2023b). Therefore, stabilized and dispersed nHAp/SDS particles could have the ability to create a barrier on shale surfaces, inhibiting clay swelling. This process will deactivate ionic compounds and reduce the shale's capacity to absorb water (Sudharsan and Khare, 2023). Therefore, it is important to understand how the nHAp/SDS test fluid affects the shale platelets for enhanced wellbore stability. This is especially true in high-temperature high-pressure (HTHP) formations and shale formations, where particles are introduced to stabilize the wellbore and improve drilling fluid efficiency (Saleh et al., 2021). Drilling in water-sensitive shale formations has raised significant concerns about potential borehole collapse. The drilling fluid systems remain a significant source of uncertainty in shale drilling because of compatibility and sedimentation problems, particularly under HTHP conditions. With several research studies in this field (Sudharsan and Khare, 2023; Blkoor et al., 2023; Abdullah et al., 2022; Luo et al., 2022; Yang et al., 2021; Huang et al., 2020), the influence of drilling fluid systems on shale drilling performance still remains uncertain. This complexity arises from the interaction between the shale formation and the drilling fluid. Hence, this study introduced a bioceramic material called nHAp/SDS to address drilling challenges like wellbore instability and enhance drilling efficiency.

This study employed nHAp/SDS particles to enhance the efficiency of the conventional KCl-WBM system when drilling through shale formations. The KCl-WBM system was developed with the addition of nHAp/SDS particles to assess its performance using a linear swell meter (LSM) at ambient temperature (25 °C) and a dynamic linear swell meter (DLSM) under HTHP conditions (80 °C). A comparison was made between the performance of nHAp/SDS drilling fluid systems, nanosilica-based drilling fluids, and the reference sample (KCl-WBM) using a series of shale stability tests. Finally, the mechanism underpinning the inhibitory performance of nHAp/SDS for enhanced wellbore stability was described.

2. Research materials and test procedures

2.1. Materials

Disodium hydrogen phosphate (Na_2HPO_4) (1.70 g/cm^3 density, 141.96 g/mol mol. wt.), SDS (1.01 g/cm^3 density, 288.38 g/mol mol. wt.), calcium carbonate ($CaCO_3$) (2.71 g/cm^3 density, 100.09 g/mol mol. wt.), sodium bentonite, caustic soda (NaOH), and KCl were acquired from QRëC, Japan through MyLab Supplier, Malaysia. The Merck Company in Germany provided additional drilling mud additives (PAC-R, PAC-LV, HPAM, XGD, biocide, antifoam agent, barite, and starch-HV). All materials were used without undergoing further purification processes. Nanosilica of average particle diameter 12 nm, 175–225 m^2/g surface area, 60.084 g/mol molecular weight, and 4.21 g/cm^3 density was acquired from Sigma-Aldrich, Selangor, Malaysia.

Synthetic materials such as nHAp and SDS particles used in this research are comparable to nanosilica as they are all derived from synthetic sources and are biocompatible. Both materials offer a significant advantage in terms of high temperature resistance. However, nHAp appears to be more thermally stable, capable of withstanding temperatures up to 800 °C without decomposing. This is advantageous for drilling fluid, as it will enhance heat transfer by improving thermal stability (Bulina et al., 2021). For its versatility, nHAp finds applications in various fields, including material science, bioceramics, biomedical engineering, and bone tissue engineering (Abidi and Murtaza, 2014). It can be used for the development of biomaterials using NPs and nanocomposites in combination with polymers or ceramics. Furthermore, nHAp demonstrates superior solubility and bioactivity compared to nanosilica. Nevertheless, it has lower surface energy than nanosilica, making it beneficial for drilling fluid systems. The high surface energy of nanosilica leads to its tendency to agglomerate in suspension compared to nHAp. While nanosilica particles offer benefits due to their atomic-scale size, nHAp can be processed to contain nanoscale particles, usually ranging from tens to hundreds of nanometers in size. The small particle size enables a larger surface area and enhanced bioavailability (Shi et al., 2009). This is the reason why nHAp particles can be highly beneficial for sealing shale nanopores.

2.2. Mineralogical composition of Endau-Rompin shale

Clay minerals exhibit a significant attraction to water, comprising approximately 50–60 wt% of the majority of shales (Abatan et al., 2016). Shales typically contain a moderate to high clay content, averaging around 57 %, according to various studies (Zhang et al., 2017; Jiang et al., 2022; He et al., 2016). Studies have shown that smectite minerals and mixed smectite and illite layers are the main reasons for clay swelling. This is because of their 2:1 arrangement and ability to exchange cations (Jiang et al., 2022). Therefore, highly reactive clay mineral with high clay contents due to its strong water affinity was selected in this study. The mineral composition of the selected shale sample was examined using an X-ray diffraction (XRD) device, following the methodology outlined by Rana et al. (2020) (Table 1). Based on the quantitative XRD analysis, it was noted that this structure contains 58.2 % clay content. The 58.2 % clay content was further categorized as follows: 1.8 % illite, 1.39 % chlorites, 2.50 % kaolinite, 18.1 % smectite, and 24.4 % illite/smectite mixed layer.

The shale cuttings used in this study were obtained from the Endau-Rompin formation in Malaysia. This research focused solely on smectite-dominated shales due to the unique properties of other clay minerals like kaolinite or illite, which can also lead to clay swelling. The classification of the clay contents indicates that the illite/smectite mixed strata are prevalent in the shale sample. It also indicates that smectites are the most common. Just like smectite, illite clay expands and weakens when saturated. Before engaging the shale with drilling muds, the pore

Table 1
Shale sample mineralogical compositions.

Component	Iron dolomite	Quartz	Calcite	Plagioclase	Potassium feldspar	Clay mineral
Amount (wt.%)	2.8	11.3	12.8	10.6	4.3	58.2

structure was characterized by scanning electron microscopy (SEM) (Hitachi SU8020, Japan). The SEM image in Fig. 1a displays a diverse array of nanopores within the shale sample, enhancing its water absorption capacity. The energy-dispersive X-ray spectrometry (EDX) scans in Fig. 1b and Table 2 show that the relative weight percentage of the shale is consistent with the shale's reported composition by Sharma et al. (2016).

2.3. Synthesis of nHAp/SDS particles

$CaCO_3$ and Na_2HPO_4 are the precursors for nHAp/SDS synthesis. They act as the building blocks for nHAp production in a ratio of 1.67. By utilizing its alkyl chains and hydrophilic head group (SO_4^{2-}), the SDS acts as an essential component in controlling the formation of nHAp crystals with specific sizes and enhancing the synthesis parameters for improved particle dispersion and stability. When $CaCO_3$ is combined with Na_2HPO_4, it results in the production of standard nHAp particles. These combinations are recognized for their exceptional chemical and thermal stabilities, distinct sorption properties, adsorption, biocompatibility, and bioactivity (Bulina et al., 2021). $CaCO_3$ plays a role in providing calcium ions that interact with $PO_4$3- groups to form calcium-phosphate (Ca/P) molecules, which are necessary for nHAp formation.

The in situ chemical precipitation route and formation of nHAp/SDS particles are presented in Fig. 2 following previous method (Bulina et al., 2021). Na_2HPO_4 powder of 68.1 g was mixed in 1000 mL distilled water at 80 °C at 600 rpm for 30 min. Under 600 rpm stirring, 80.1 g of $CaCO_3$ solution was fed slowly into the solution using a graduated burette. This ensured that the $CaCO_3$ dissolved properly. A 200-mL SDS solution (prepared by dissolving 10 g of SDS in 300 mL of distilled water) was introduced into the mixture while it was being mixed. A constant pH of 10 tuned with NaOH (0.625 M) was used, and the solution was agitated at a rotating speed of 600 rpm to make a white suspension. To avoid thermal shock to the formed product, it was naturally cooled in a fume hood (Koroleva et al., 2020). After the precipitates had cooled, they were centrifuged at room temperature for 20 min at 6000 rpm and then rinsed three times with distilled water to get rid of any impurities. The sample was made dry using an air-drying kiln method for 1440 min at 60 °C, pulverized, and analyzed using different tools.

2.4. Characterization of nHAp/SDS material

The particle size distribution (PSD) of the nHAp/SDS particles was determined using the Malvern Instruments ZetaSizer version 11, Malvern, UK. At 25 °C, a Perkin-Elmer FTIR 2000 spectrophotometer was used for scanning from 4000 to 400 cm^{-1} at 4 cm^{-1} resolution to find out how the bonds in nHAp/SDS are set up and what functional groups they have. A 120-kV TEM (transmission electron microscope), HT7700 Hitachi, Tokyo, Japan, was used to record the structure of nHAp/SDS in an aqueous solution. The thermal stability from 20 to 1000 °C at 10 °C/min under nitrogenous conditions was tested using a differential thermal thermogravimetric analyzer (TGA/DTG) (TGA Model Q5000, USA). Using 40 kV, 40 mA, and radiation 1.5418740A Cu-Kα (α = 0.154 nm), an XRD instrument from Advance D8-Bruker, AXS, Germany was used to measure the nHAp/SDS crystalline state. It was scanned between 20 and 60° (2θ/0.5° min), and the XRD pattern and phase formation of nHAp/SDS were confirmed.

Table 2
EDX data of shale sample before testing.

Element	C	O	Al	Mg	K	Si	Fe
Relative (wt.%)	26.73	41.08	9.86	1.04	1.12	15.77	4.08

2.5. Mud-Making tests and measurements

The drilling muds were produced according to API RB 13B-2 (2019) recommended standards. The base fluid sample (KCl-WBM) was prepared by stirring 1.5 wt% sodium bentonite, 4.0 wt% KCl, 0.4 wt%, PAC-LV, and 0.06 wt% NaOH in 310 mL tap water at 1100 rpm for 40 min to produce 350 mL of WBM. The KCl-WBM was mixed with nHAp/SDS concentrations of 0.5, 1.0, 1.5, and 2.0 wt% to make nHAp/SDS test fluids. Nanosilica test fluids were formulated using the same steps. The rheological properties were measured using a Fann 35 SA viscometer. During this experiment, the drilling fluids were stirred at different shear rates ranging from 3 to 600 rpm, and the corresponding shear stress was recorded. The viscosities (AV and PV), yield point (YP), and gel strength (GS at 10 s and 10 min) were estimated using Eqs. (1) – (5). API filter meter (series 300, USA) was used to measure the fluid loss (API FL) after introducing the 350 mL drilling fluids at 100 psi and room temperature. For 30 min, the filtrate was collected in a graduated cylinder at predetermined intervals. The thickness of the deposited filter cake (API FCT) was measured using a vernier caliper. For consistency, Fann viscometer and API filter press tests were undertaken two times for each fluid system, and the average data were recorded.

$$AV(cP) = \frac{\theta_{600}}{2} \quad (1)$$

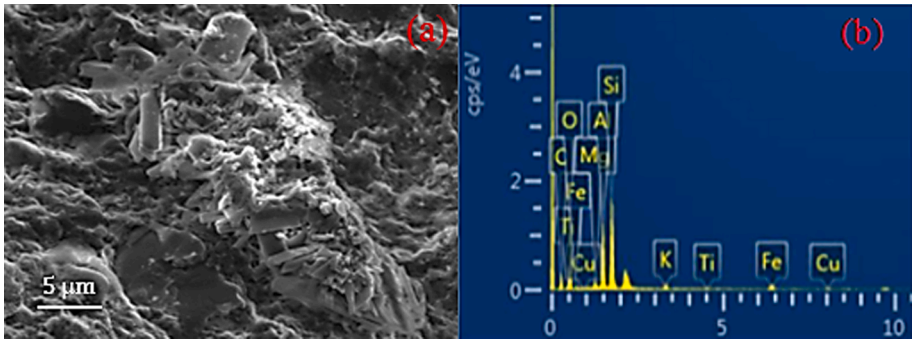

Fig. 1. Shale sample before testing (a) SEM image and (b) EDX data.

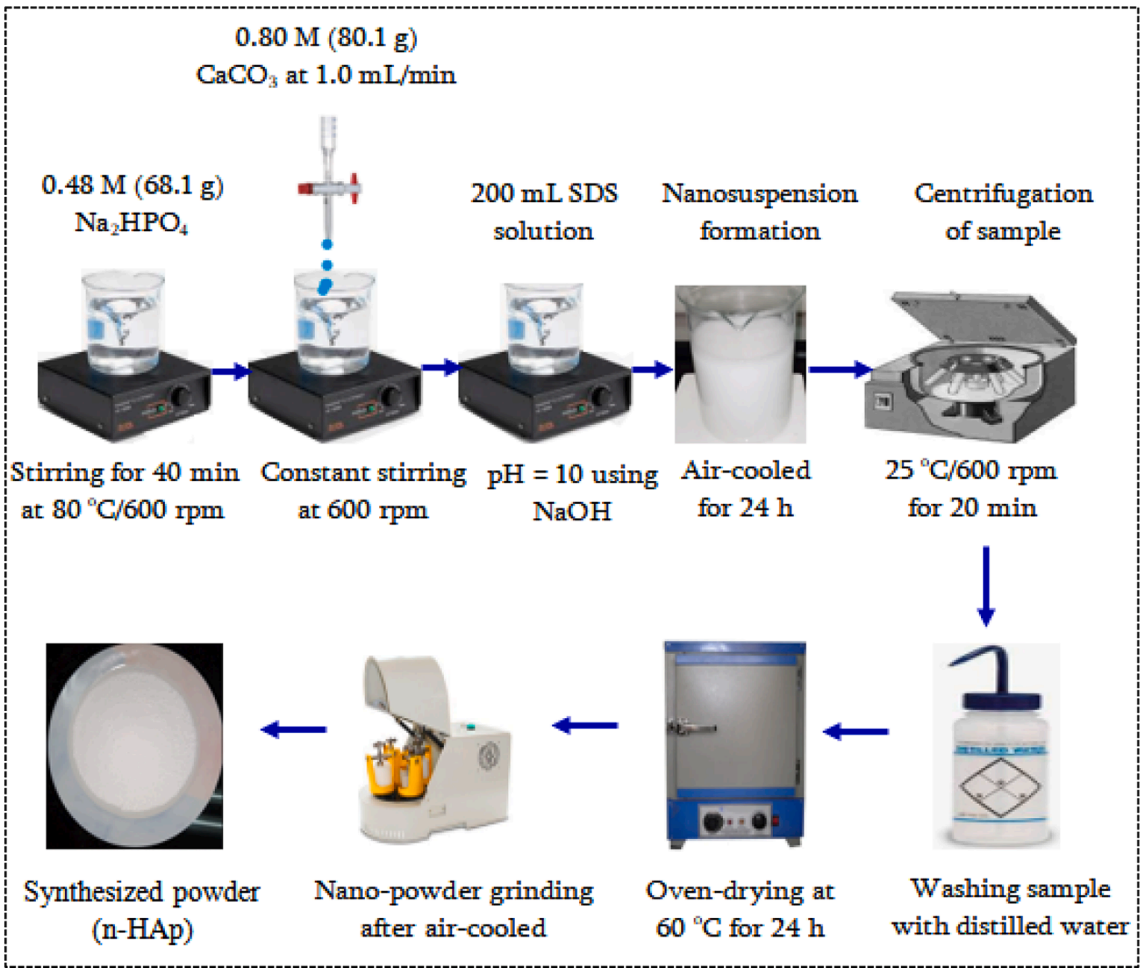

Fig. 2. Synthesis of nHAp/SDS particles.

$$PV(cP) = \theta_{600} - \theta_{300} \tag{2}$$

$$YP\left(\frac{lb}{100ft^2}\right) = \theta_{300} - PV \tag{3}$$

$$GSat10s\left(\frac{lb}{100ft^2}\right) = \theta_3 after 10s \tag{4}$$

$$GSat10m\left(\frac{lb}{100ft^2}\right) = \theta_3 after 10min \tag{5}$$

2.6. Methods of shale stability tests

2.6.1. Shale hot-rolling dispersion test

A hot-rolling dispersion test was used to determine the inhibitory effects of KCl-WBM, nanosilica, and nHAp/SDS on the dispersion of shale cuttings. The injected drilling fluids follow the same formulation used in Section 2.4. The test began with crushing and sieving the shale samples obtained from Malaysia's Endau-Rompin formation, using sieve apertures ranging from 2.30 mm to 3.15 mm. An ageing cell containing 350 mL of inhibitory drilling fluids was filled with 30 g of the sieved shale cuttings, and the top was securely shut. The aging cell was placed into the Fann Model 704ET-4 compartment roller ovens, where the mixture was subjected to a temperature of 65 °C for 16 h. The shale sample was removed and cooled to room temperature after ageing. It was washed with deionized water and sieved using a 40-mesh sieve after cooling. The sieved cuttings were recovered and dried at 100 °C for 4 h. After drying, the final mass was measured, and the retention percentage was determined from the initial mass. The dispersion recovery rate (R) of the final mass of the cuttings (W_c) was calculated using Eq. (6). This test was conducted twice for consistency, and the average values were reported. A good inhibitor is the fluid sample with a high retention percentage. Repeating the steps with temperatures set at 105 °C and 120 °C helped analyze the impact of higher temperatures on the shale sample disintegration and the effectiveness of the drilling fluids in preventing it. The study's use of temperatures of 105 °C and 120 °C could be deemed adequate since higher temperatures increase the kinetic energy of shale particles, causing them to become unstable (Jia et al., 2019).

$$R(\%) = \frac{W_c}{30} \times 100 \tag{6}$$

2.6.2. Linear swell meter (LSM) test

An LSM was used in this experiment to determine the performance of inhibitive drilling fluid systems in drilling clay-dominated shale formations at room temperature (25 °C). The injected drilling fluids follow the same formulation used in Section 2.4. This test followed the steps outlined by Zhong et al. (2020) and Lalji et al. (2023). For this experiment, a conventional KCl-WBM system was set up as the control mud. Eight different sets of inhibitive mud systems (0.5 wt%, 1.0 wt%, 1.5 wt %, and 2.0 wt%) consisting of nHAp/SDS and nanosilica were tested. Initially, tap water was used to engage with the shale sample as a foundation for assessing the effectiveness of the KCl-WBM system because of the significant incompatibility of water with shale drilling. The average findings were reported after the tests were repeated to ensure accuracy. The collected cuttings were crushed using a 30-mesh

shale grinder and then screened with deionized water to remove any contaminants. The powdered samples were dried for 4 h at 100 °C in an oven and vacuum-dried for 3 h. Utilizing a hydraulic compactor, the shales were compressed at 10,000 psi for 90 min to create shale plugs measuring 15 mm in height and 25.4 mm in diameter, with a precision of 0.01 mm.

A total of 10 shale plugs were produced. Every 10 min, the compactor cell pressure was monitored and gradually raised to 10,000 psi until it stabilized. After adjusting the 15-mm shale plugs in a core holder, they were transferred to the LSM cell's measurement head in the shale chamber, where they could only expand vertically. The four cells of LSM were calibrated using the recommended calibration procedure. The plugs were placed in the LSM cell. In each cup, 20 mL of drilling fluid was introduced to interact with the shale plug. The shale plugs were tested simultaneously with the drilling fluids for 48 h. The LSM test uses linear displacement response when the shale plugs are in contact with the drilling fluids to assess the expansion of the shale plugs. The rate of expansion of the shale plug was determined using Eq. (7), where the initial height of the shale plug is 15 mm. The Eq. (7) is defined as the difference in the expanded height of the plug from the original height of the plug.

$$\text{Linear swelling rate}\,(\%) = \frac{(\text{Difference in shale plug height})}{(15)} \times 100 \qquad (7)$$

2.6.3. Dynamic linear swell meter (DLSM) test

The swelling characteristic of the Endau-Rompin formation due to increased temperature was analyzed using the HTHP OFITE DLSM (Model 150–80-230 V, USA). The test procedures follow those outlined by Lalji et al. (2023) and Barati et al. (2017) for DLSM. The process of preparing the shale plugs for the LSM test was repeated, resulting in the production of 10 additional shale plugs through hydraulic compaction. The injected drilling fluids follow the same formulation used in Section 2.4. The shale plugs were exposed to the test drilling fluids for 48 h at 80 °C in the DLSM cup assembly, and the swellings were measured over time. DLSM can test up to four samples simultaneously. The sample was left to swell for 48 h before it was taken out. The fundamental idea behind the equipment is to capture any variation in the sample's height as it interacts with the fluid. A linear variable transducer built into the equipment records the height variation. The more ions migrate inside the shale platelets, the more swelling will be observed over time. The impact of stress and pressure was not examined during the tests because DLSM primarily operates by inferring the alteration in height of the sample using a transducer.

2.6.4. Shale pore structure characterization and contact angle measurements

A SEM (Hitachi SU8020, Japan) analysis test was conducted on the shale's pore structure after nHAp/SDS inhibition. The results indicated a collaborative relationship between the shale stabilizers and the shale pores. The effectiveness of nHAp/SDS in shale inhibition was clearly demonstrated in the pore structure images. Changing the surface wettability is one of the most significant techniques for mitigating the negative impacts of clay's hydrophilic properties and water invasion (Yue et al., 2018). The contact angle θ (theta) test is the most direct approach for determining surface wettability. The water contact angle was determined using the hanging drop form technique with a DSA25 contact angle tester (Luo et al., 2022). Following the immersion of the shale specimen in drilling mud for 24 h, the shale samples were subjected to 2 h of blast drying at 70 °C. The measurements were taken using the contact angle drop shape meter (DSA25 analyzer). A syringe filled with water was used to carefully administer a drop onto the specimen as photos were taken of the chip. The outer diameter of the needle measures 0.30 mm, with an inner diameter of 0.22 mm. For a precise view of the centre drop, angled needles were necessary. A water droplet was captured on the chip, and the contact angle of each drilling fluid was assessed. Luo et al. (2022) thoroughly describe these test methodologies.

2.6.5. Measurement of zeta potential of shale core with nHAp/SDS and nanosilica

The ZP also verified the electrical stability of the shale stabilizers and pores. The ZP, an interfacial parameter that accounts for electro-kinetic charge, is crucial to understanding solid materials and their charge and adsorption properties (Elochukwu et al., 2017). The most effective way to determine a NP's surface charge is by using ZP. According to Hoxha et al. (2016), surface charge is the electrical potential difference between the inner and outer surfaces of NP colloid. To evaluate the level of interaction between the NPs and shales, ZP measurements were carried out on unaltered shale-thin parts exposed to the drilling fluids, as well as on nanosilica and nHAp/SDS aqueous dispersions. Electrophoresis was used to quantify the solid surface ZP in aqueous solutions using a specially constructed Malvern surface ZP cell. Thus, it was used to study the NPs (nanosilica and nHAp/SDS)-shale charge interactions. The pH range used for the experiment was from 0 to 14, titrated with NaOH and HCl solutions, each with a concentration of 0.5 M. The temperature employed remained fixed at 25 °C. A detailed measuring approach is given in the Hoxha et al. (2016) study. Nanosilica was dispersed before ZP measurements. 0.05 wt% NaOH was combined with nanosilica in a 200-mL container with 50 mL tap water. To prevent particle agglomeration, the nanosilica dispersion was ultrasonicated for 60 min using the Probe sonicator, BMS-750 T.

2.7. HTHP suspension stability test of nHAp/SDS-based drilling muds

To determine the suspension stability of nHAp/SDS test fluids, drilling fluid formulation steps from Section 2.4 were used to formulate nHAp/SDS-based drilling muds with 0.5, 1.0, 1.5, and 2.0 wt% concentrations. The suspensions were stirred energetically for 10 min and sonicated for 5 min using a BMS-750 T Probe sonicator. Images of the suspensions in small glass vials (10 mL) were captured to assess the sedimentation over time following a 16-h ageing period at 120 °C in a 4-roller oven. The sedimentation stability was monitored for 144 h (6 days) to assess the physical fluid suspension stability. The sedimentation ratio was calculated as the ratio of the sediment height (H_s) to the vial height (H_v) (i.e., the initial fluid height). The ratio was shown on a time-dependent graph. The suspensions' HTHP rheological characteristics were measured using an OFITE HTHP viscometer #900, and their filtration properties were measured with an OFITE HTHP dynamic filter press #130–74, following the techniques outlined in Section 2.4.

2.8. Compatibility test of nHAp/SDS test fluids

Two different types of prepared drilling muds, water-based drilling fluid (WBDF) and high-performance drilling fluid (HPDF), were prepared to ascertain the compatibility of nHAp/SDS with the other common drilling fluid additives (Table 3). This test followed the outline steps described by Barati et al. (2017). The drilling muds were tested for rheological and filtration properties after adding 2 wt% nHAp/SDS,

Table 3
Drilling mud formulation for compatibility test of nHAp/SDS test fluids.

	Preparation	
WBDF	Tap water (420 mL) + NaOH (0.2 g) + starch-HV (8.3 g) + PAC-R (2.41 g) + XGD (1.25 g) + biocide (0.3 mL) + antifoam (0.1 mL) + barite (up to 1.066 g/mL).	WBDF + 2 wt% nHAp/SDS
HPDF	Tap water (420 mL) + NaOH (0.2 g) + starch-HV (8.3 g) + PAC-R (2.41 g) + HPAM (1.10 g) + PAC-LV (1.12 g) + XGD (1.25 g) + KCl (15 g) + biocide (0.3 mL) + antifoam (0.1 mL) + barite (up to 1.066 g/mL).	HPDF + 2 wt% nHAp/SDS

according to the steps described in Section 2.4. The drilling muds were aged for 4 h at 70 °C using a hot rolling oven running at 22 rpm. In accordance with API-suggested practice on the rheology and hydraulics of oil-well drilling fluids, the filtration and rheological characteristics were measured (API RP 13D, 2023).

3. Results and discussions

3.1. nHAp/SDS findings from various characterizations

The characterization results of nHAp/SDS are shown in Figs. 3 and 4. TEM revealed the structure of synthesized nHAp/SDS particles (Fig. 3a and b). As shown in Fig. 3a and b, the synthesis process produced dispersed nHAp/SDS crystals with rod-like lengths of 20–160 nm and diameters of 10–30 nm. Origin-package was used to investigate the rods' dispersion after measuring their diameters and lengths using J-icon (Fig. 3b). These results show that nHAp/SDS rods average 80.0 nm long and 18 nm wide. The rod length mean to diameter ratio gives an aspect ratio of 4.5 nm (Fig. 3b), which matches that of a recent study by Ngouangna et al., (2022a). In Fig. 3c, nHAp/SDS had a unimodal distribution with a 105.7 nm peak frequency and a 70–600 nm diameter. The distribution standard deviation and the average diameter are 38.3 nm and 110.4 nm, respectively. Diameters D_{90}, D_{50}, and D_{10} are 189.8, 91, and 22.2 nm, respectively. PSD data matches TEM analyses, and the particles were within the nano-range diameter for drilling operations.

Fig. 3d displays the XRD analysis of nHAp/SDS powder components and their crystalline peaks. The laboratory diffraction peaks of nHAp/SDS suggest the presence of hexagonal HAp crystals, as reported by Bulina et al. (2021). The diffraction patterns align with HAp, specifically reference HAp (ICDD® 9–0432) and other sources. The peaks are consistent with HAp crystals formed using the precipitation method described by Koroleva et al. (2020). The XRD analysis indicated that the HAp did not transform into other phases like tricalcium phosphate or calcite when dried at 60 °C, indicating successful product formation (Jamarun et al., 2023). The XRD peak patterns for [2 1 0], [1 3 0], and [1 3 2] show sharp peaks, suggesting that the nHAp/SDS crystals synthesized are well-developed, pure, and maintain their crystallinity (Koroleva et al., 2020). The peak patterns indicate a hexagonal structure for the nHAp/SDS. Elemental compositions in Fig. 3d indicate that the nHAp/SDS particles consist of SDS, calcium, and phosphorus, as shown by the blue percentages. These particles exhibit an exceptional stoichiometry ratio, similar to the natural HAp ratio of 1.67. The final product contains Carbon (C), Sulphur (S), and Sodium (Na) elements, which are not present in the original HAp formula.

Fig. 4a demonstrates the high thermal stability of nHAp/SDS up to 750 °C, maintaining 73 % of its original structure. It is well-suited for drilling into deeper formations. The derivative weight curve (DTG) shows three peaks, which suggest that the nHAp/SDS breaks down in three different ways. The particles' stability was reduced at 850 °C. These findings are consistent with previous research by Bulina et al.

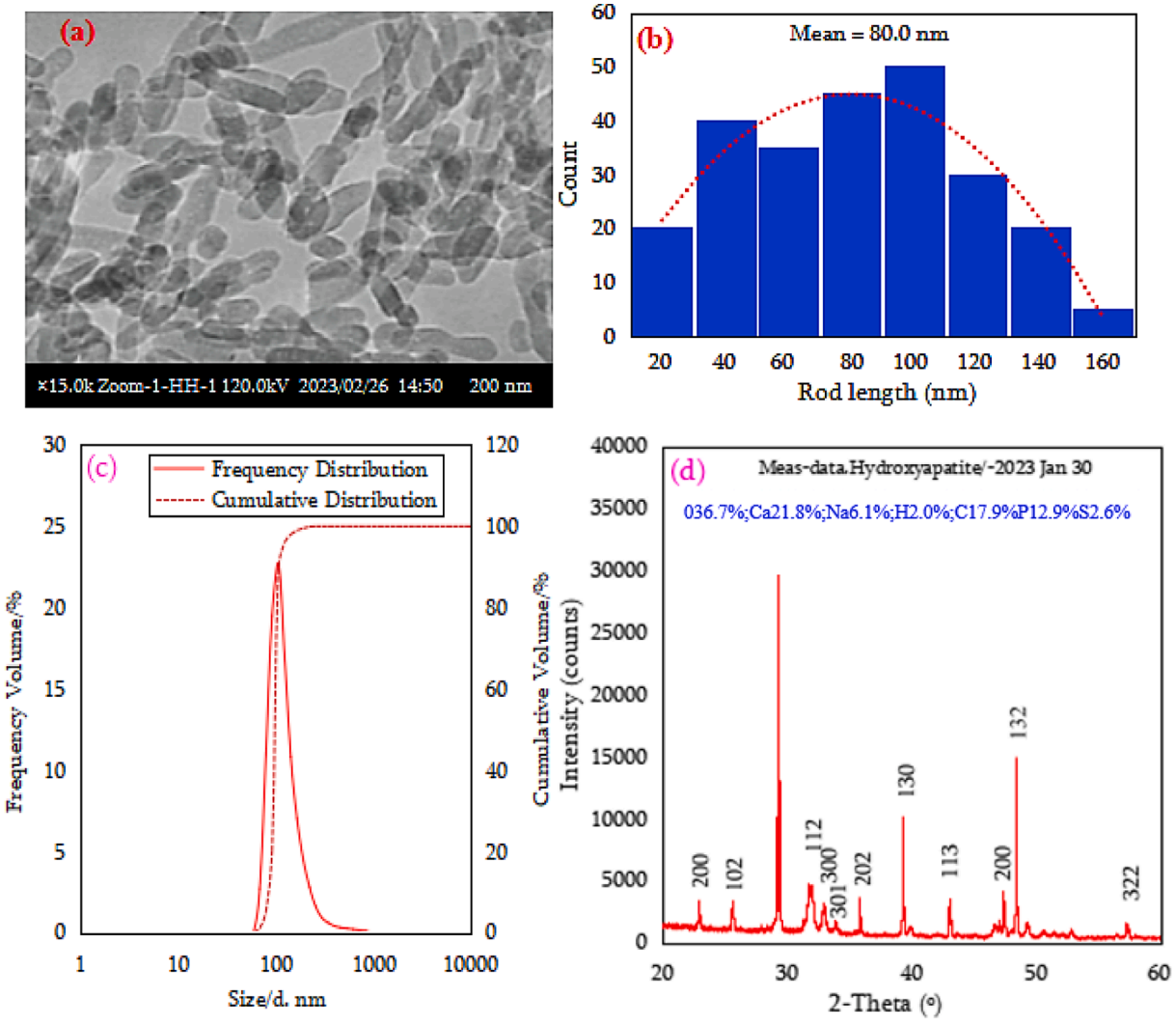

Fig. 3. Nhap/sds (a) tem microstructure, (b) particles rod length distribution, (c) psd, and (d) xrd data.

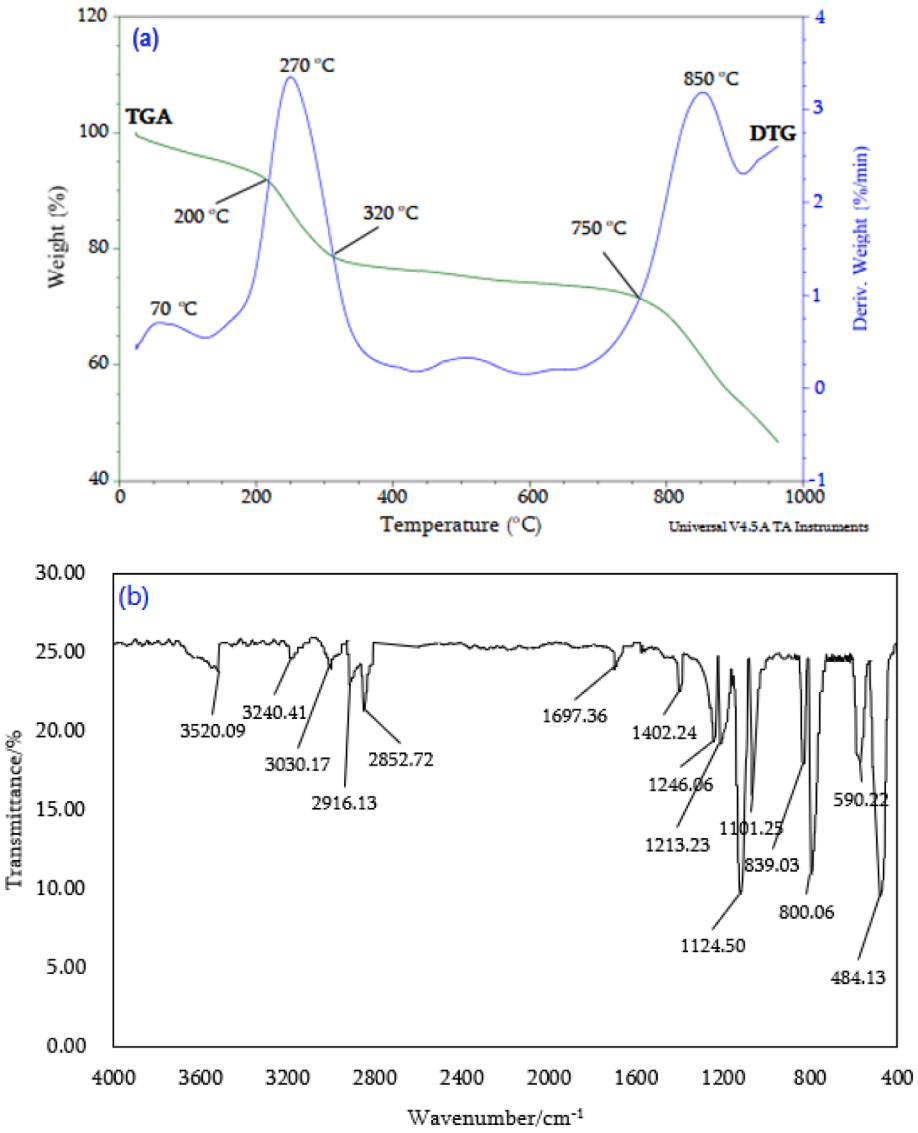

Fig. 4. Nhap/sds (a) tga/dtg curves and (b) ftir spectra.

(2021) and Koroleva et al. (2020). The TGA finding also confirms the presence of SDS molecules in the nHAp/SDS structure. When heated to 850 °C, the phosphate and carbonate components of the particles in the nHAp/SDS layer undergo complete decomposition. As a result, the nHAp/SDS particles lose stability at temperatures up to 850 °C.

Based on Fig. 4b, it was found that various functional groups were part of the designed nHAp/SDS. The peaks at 3520.09, 3240.41, and 3030.17 cm^{-1} are a result of the stretching vibrations of the –OH groups on the surface of nHAp/SDS (Prasad et al., 2023; Ngouangna et al., 2022a). The assignment reaches 2916.13 and 2852.72 cm^{-1} for the hydrophobic tail of SDS, while 1697.36, 1246.06, and 800.06 cm^{-1} are associated with the hydrophilic sulphate head group (SO_4^{2-}) of SDS (Koroleva et al., 2020). The peaks associated with the carbonate group (CO_3^{2-}) of nHAp/SDS were observed at 1402.24, 1124.5, and 839.03 cm^{-1} (Córdova-Udaeta et al., 2021). The phosphate group (PO_4^{2-}) in nHAp/SDS is indicated by the peaks at 1101.25, 590.32, and 484.13 cm^{-1} (Bulina et al., 2021). The FTIR analysis highlights the effect of SDS modification on n-HAp, as illustrated in Fig. 4b. The results show that the nHAp/SDS that was formed is made up of SDS, $CaCO_3$, and Na_2HPO_4, which are the same elements that were found in the XRD analysis.

3.2. PV, AV, GS, YP, API FCT, and API FL of nanosilica and n-HAp/SDS-based drilling muds

Table 4 shows the results of KCl-WBM systems formulated with different concentrations of nanosilica and nHAp/SDS at room temperature (25 °C). The rheological properties of nHAp/SDS outperform those of nanosilica. The rheological data indicated that incorporating nHAp/SDS and nanosilica into the KCl-WBM led to enhanced rheological properties as the concentration increased. The most significant PV increase was observed with 2.0 wt% of nHAp/SDS, resulting in a remarkable 90 % increase compared to the KCl-WBM. Using the same quantity of nanosilica resulted in a change in PV from 10 to 17 cP, representing a 70 % increase. KCl, in combination with bentonite, can help boost the viscosity of water solutions. The presence of KCl in the drilling fluid increased the ionic strength of the base mud, which improved the electrostatic attraction between the water layers. As a result, there was an enhancement in the intermolecular forces among the water molecules (Sehly et al., 2015).

The nHAp/SDS particles excel at adsorption, enabling them to interact with polymer–clay adsorption sites in the KCl-WBM. This phenomenon enhances the integrity of the polymer–clay matrix of the muds by reducing the propensity of particles to separate, thus leading to an

Table 4
Nanosilica and nHAp/SDS filtration and rheological properties at 25 °C (unaged muds) using the mud formulation in Section 2.4.

Drilling mud formulations		θ_{600}	θ_{300}	Gel (10 s/10 min) (lb/100ft^2)	PV (cP)	AV (cP)	YP (lb/100ft^2)	FL (mL)	FCT (mm)
WBM	0.0 wt% nHAp/SDS	30	20	3.5/4.5	10	15	10	7.9	0.88
WBM	0.5 wt% nHAp/SDS	35	23	3.0/4.0	12	17.5	11	6.4	0.81
WBM	1.0 wt% nHAp/SDS	40	26	4.0/5.0	14	20	12	5.8	0.72
WBM	1.5 wt% nHAp/SDS	46	30	5.5/7.5	16	23	14	4.7	0.63
WBM	2.0 wt% nHAp/SDS	54	35	5.0/8.0	19	27	16	3.1	0.47
WBM	0.5 wt% Nanosilica	33	22	3.0/3.5	11	16.5	11	7.3	0.84
WBM	1.0 wt% Nanosilica	35	23	4.5/6.0	12	17.5	11	6.6	0.80
WBM	1.5 wt% Nanosilica	41	27	4.0/7.0	14	20.5	13	5.4	0.69
WBM	2.0 wt% Nanosilica	48	31	5.0/6.5	17	24	14	4.6	0.58

increase in the viscosity of the mud (Naeimavi et al., 2020). In addition, the study by Elochukwu et al. (2017) demonstrates that incorporating nanosilica into a drilling mud system enhances the rheological properties. It is possible that the nanosilica's small size of 12 nm contributes to its large specific surface area per unit volume. The internal friction between the mud particles and nanosilica particles in suspension is strengthened (Saleh et al., 2021).

Table 4 illustrates the slight gel structure differences among the various fluid samples for both the 10-s and 10-min measurements. The gel structure remained consistent over time. This feature is very desirable, as the gel can effectively retain the suspension of drilled particles even in situations where there is no flow. Additionally, breaking the gel during flow can help restart the flow after extended periods of inactivity (Oseh et al., 2019). This study highlights the rheological values that offer drilling fluid benefits for drilling operations by decreasing power demands on pumps, ultimately enhancing pump and drilling efficiency (Mao et al., 2015). Additionally, filtration properties result show that incorporating nHAp/SDS into KCl-WBM improves its effectiveness as a fluid loss control agent compared to nanosilica (Table 4). As the concentrations of both nHAp/SDS and nanosilica increased, there was a significant decrease in water loss observed in the base mud. Nanosilica did not perform as well in managing fluid loss compared to nHAp/SDS. Concentrations of nHAp/SDS (0.5–2.0 wt%) led to a decrease in API FL by 19–61 %, whereas nanosilica concentrations (0.5–2.0 wt%) resulted in an 8–42 % reduction compared to the KCl–WBM system.

According to the data in Table 4, the mud systems that were prepared had filter cakes smaller than 2.0 mm with minimal variation. When nHAp/SDS is added to the KCl-WBM, it improves its coating properties. This effectively seals the pores of the filter paper to block water from passing through (Saleh et al., 2021). A thin mud cake of nanosilica was inserted between the formation under drilling and the wellbore to reduce drilling fluid water loss (Huang et al., 2018). The shale stabilizers under investigation, nHAp/SDS and nanosilica, possess rheological and filtration characteristics that are beneficial for drilling fluids and oilfield operations. Whether the properties of nHAp/SDS particles remain consistent at all depths in the formation being drilled determines their effectiveness in preventing clay expansion during shale drilling. Due to the synergistic sealing effect and cost savings, 2.0 wt% of the nHAp/SDS shale inhibitor is the best concentration. Furthermore, the nHAp/SDS and nanosilica mud formulations are more likely to prevent clay swelling at this concentration.

3.3. Shale cuttings hot-rolling recovery performance

Fig. 5 displays the findings from experiments conducted to study the hot-rolling dispersion of shale particles mixed with drilling fluids. According to the data in Fig. 5, the shale specimen's recovery rate after being hot-rolled at 65 °C and tested with tap water was 39.2 %. This observation underscores a remarkably low recovery rate for the shale specimen. Through the utilization of base mud containing KCl, a notable enhancement was observed in the shale specimen recovery rate, reaching 63.3 %. It has been shown in the past that potassium ions (K^+) can replace sodium ions (Na^+) in the montmorillonite (Mt) interlayer. When they are hydrated, they become smaller, which lowers the hydration energy (Steiger, 1982). According to Naeimavi et al. (2020), decreasing the thickness of the hydration shell enhances the electrostatic interaction between the clay platelets and counterions. As a result, there was improved inhibition of water absorption and the dispersion of shale in the base mud.

However, the use of nHAp/SDS led to a more pronounced reduction

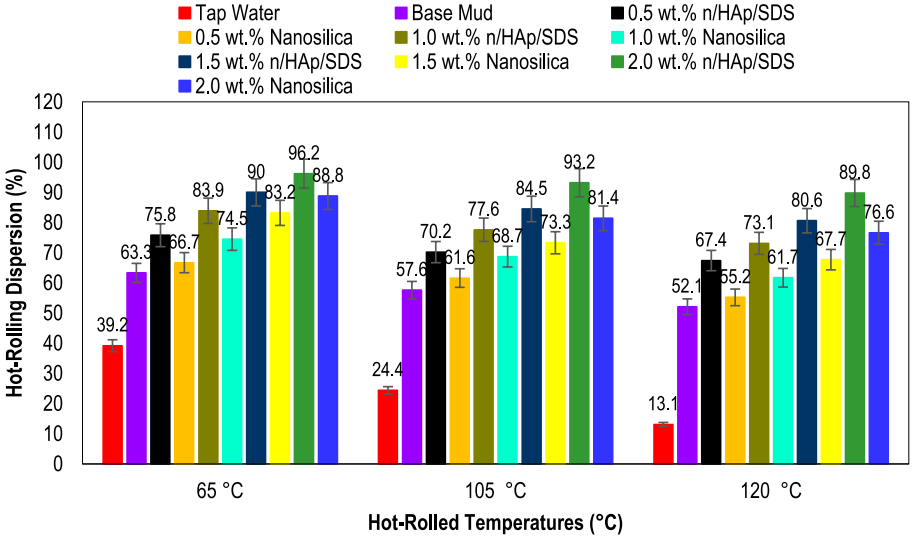

Fig. 5. Shale hot-rolling dispersion of base mud with 0.5, 1.0, 1.5, and 2.0 wt% of the shale stabilizers at different temperatures of 65, 105, and 120 °C (drilling fluids were formulated according to the recipe in Section 2.4).

in shale cutting dispersion. The K^+ exchange works together with nHAp/SDS complexes to inhibit shale hydration and dispersion. The contact angle test results are shown in Fig. 9. They show that the nHAp/SDS material is hydrophobic and can inhibit water from entering the clay (Luo et al., 2022). Through the addition of different concentrations (0.5, 1.0, 1.5, and 2.0 wt%) of nHAp/SDS, the shale recovery rate of the base mud improved to 75.8 %, 83.9 %, 90 %, and 96.2 %, respectively. Similarly, using the concentrations of nanosilica improved the shale recovery rate. Specifically, the recovery rates for nanosilica were 66.7 %, 74.5 %, 83.2 %, and 88.8 % for the specified concentrations, respectively. A recent study by Zaire and Nasiri (2021) highlighted the substantial impact of pure nanosilica particles in inhibiting shale dispersion and hydration. This study highlights the unique characteristics of nanosilica particles, such as their small size of 12 nm, large specific surface area ranging from 175 to 225 m^2/g, and high surface energy. These attributes help in plugging shale pores (Sudharsan and Khare, 2023; Oseh et al., 2020a).

It has been noted that increased hot-rolling temperatures can diminish the effectiveness of drilling fluid formulations in inhibiting shale cutting dispersion. Studies have indicated that shale disintegration can be determined at temperatures between 25 °C (Yang et al., 2019) and 160 °C (Jia et al., 2019) for a duration of 16 h. Higher temperatures elevate the kinetic energy of shale particles, causing them to become unstable (Jia et al., 2019). The impact of high temperatures on the dispersion of shale cuttings was measured at 105 °C and 120 °C to evaluate the prolonged exposure of the shale to the test fluids for 16 h. The findings presented in Fig. 5 indicate that increasing temperatures negatively impact shale stability. Shale recovery rates decline as the temperature increases. An increase in temperature results in a recovery rate of 24.4–13.1 % for tap water and 57.6–52.1 % for base mud. The recovery rates of hot-rolled shales for both nHAp/SDS and nanosilica increase with higher concentrations. Testing the fluids of nHAp/SDS showed higher recovery rates in comparison to nanosilica, the base mud, and tap water. The hot-rolling recovery rates of nanosilica range from 81.4 to 55.2 %, while those of the nHAp/SDS test fluids are between 93.2 and 67.4 % as the temperature increases from 105 to 120 °C. When the nHAp/SDS and nanosilica test fluids were introduced, the change in shale cuttings' hydrophilic properties at high temperatures prevented the particles from effectively interacting with the shale surface or entering the interlayer voids to hinder the shale dispersion (Jia et al., 2019).

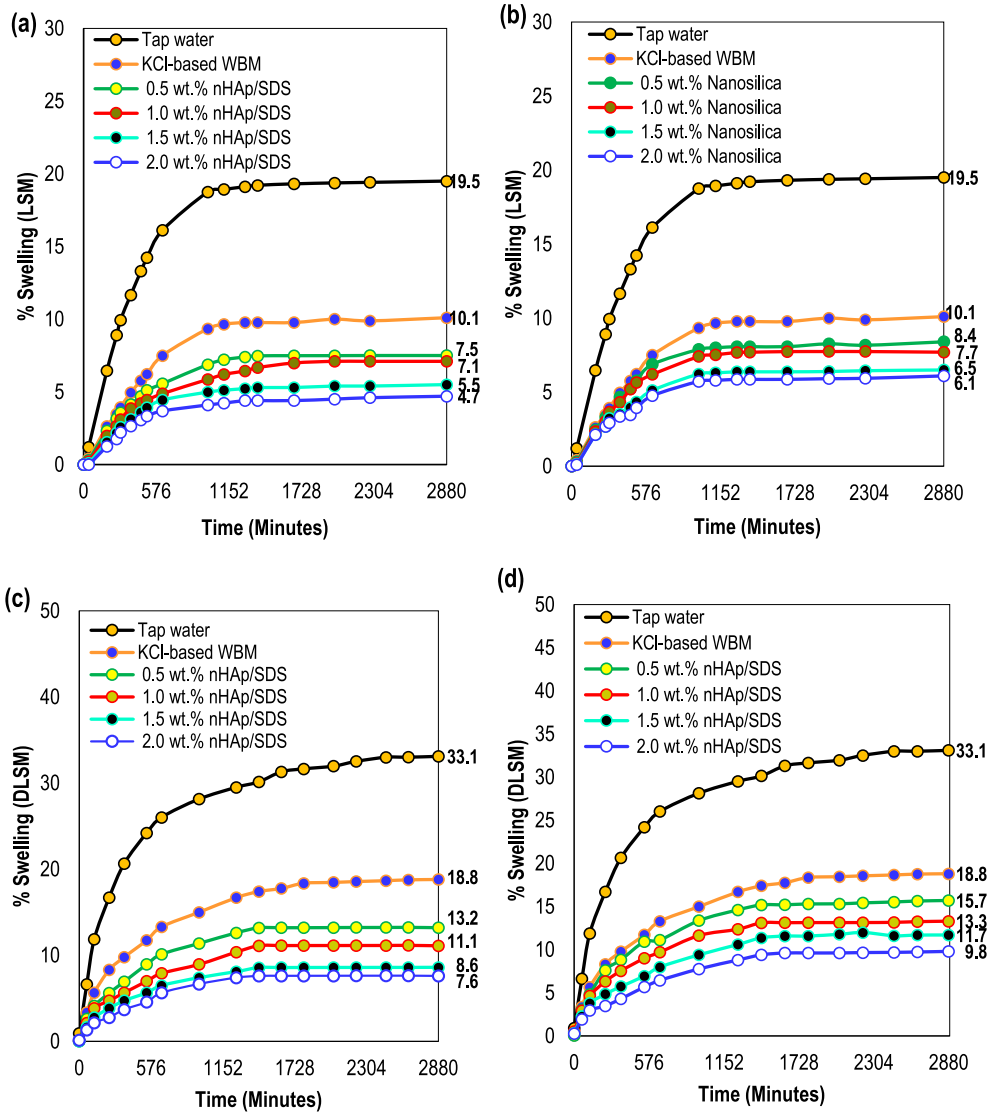

Fig. 6. Shale plug swelling in different shale inhibitors: (a) nHAp/SDS, (b) Nanosilica (a, b: LSM-25 °C), (c) nHAp/SDS, and (d) Nanosilica (c, d: LSM-80 °C) (drilling fluids were formulated according to the recipe in Section 2.4).

3.4. Inhibitive drilling fluid performance on shale swelling using LSM and DLSM

Shale cores from the Endau-Rompin formation in Peninsular Malaysia were utilized in both the LSM and DLSM tests. The XRD analysis presented in Tables 1 and 2 suggests that the shale sample has a high capacity for water absorption and expansion due to its predominant composition of smectite-rich clay and illite (Table 2). Fig. 6a and b display the linear swelling curves for tap water (reference sample), WBM with KCl, and WBM with four different weight concentrations of nHAp/SDS and nanosilica tested using LSM at room temperature (25 °C). Clay expanded when exposed to tap water for the full 48 h, resulting in a 19.5 % increase in the shale plug's volume. 10.1 % of the shale plug experienced swelling when KCl-WBM was combined with the clay in the shale, as indicated by the LSM used to calculate the swelling percentage. It indicates that the shale plug swelling was reduced by 48.2 % after being in contact with the base mud for 2880 min. As water is absorbed by the shale and hydrogen ions (H^+) migrate into the shale formation, the clay expands, causing the rock to swell and its structure to weaken. This interaction frequently results in wellbore instability, which can threaten the wellbore's integrity (Rana et al., 2020; Oseh et al., 2020b).

Using drilling fluid with the appropriate clay swelling inhibitors can help address instability issues triggered by shale formations. According to Steiger (1982), the linear swelling test shows that KCl is a highly effective conventional clay swelling inhibitor for shale problems. A small amount of KCl (4 wt%) was used in this study. This made it possible for K^+ to move through the spaces between the layers of clay and attach to the surface of the shale because it had less hydration energy. This hindered the shale from absorbing a significant amount of water (Sehly et al., 2015). Furthermore, K^+ ions possess significant cation exchange capacity, enabling them to adhere to the shale surface and engage with the ions present on the shale sheets. By replacing ions in different layers of the clay structure, the overall charge of the clay is increased. This makes the positive charge on the surface of the shale increase as well (Sehly et al., 2015). Adsorbing positive ions like K^+, Na^+, Si^{4+}, and Ca^{2+} onto the surface of shale sheets can prevent clay swelling (Steiger, 1982). Therefore, the nanoscale openings in shale are filled with KCl, but not completely due to the size mismatch between KCl and the shale nanopores.

When nHAp/SDS (Fig. 6a) and nanosilica (Fig. 6b) concentrations were used as injected fluids, the shale plugs exhibited swelling curves comparable to tap water and KCl-WBM, with a more pronounced decrease in swelling curves as weight concentrations increased. Following a 48-h contact period with shale-nanosilica test fluid, the swelling rates of the shale plugs decreased to 8.4 %, 7.8 %, 6.5 %, and 6.1 % with varying nanosilica concentrations. Overall, the nanosilica injected fluids with varying concentrations significantly decreased the reactive clay content compared to tap water (Fig. 6b). Furthermore, the inclusion of various weight concentrations (ranging from 0.5 to 2.0 wt %) of nanosilica decreased the swelling of the shale plug by 16.8–39.6 % in comparison to the KCl-WBM test fluid. Injecting nHAp/SDS test fluids into the system significantly decreased the expansion of the submerged shale plug during the LSM test (Fig. 6a). After 2880 min of testing, different amounts of nHAp/SDS were added to the shale plugs, resulting in reduced swelling rates of 7.5 %, 7.1 %, 5.5 %, and 4.7 % based on the initial plug height. When compared to the KCl-WBM, the nHAp/SDS significantly enhanced the inhibitive performance of the mud by 25.7–53.4 % after 48 h of contact time. Furthermore, the concentrations of nHAp/SDS at 0.5, 1.0, and 1.5 wt% demonstrated reductions of 61.5 %, 63.7 %, and 71.8 %, respectively, in comparison to the reference sample (tap water) (Fig. 6a). According to the findings in Fig. 6a, using nHAp/SDS at 2.0 wt% led to a 75.9 % decrease in reactive shale compared to tap water and KCl-WBM, which showed a 53.4 % reduction. It is evident that nHAp/SDS has notably decreased the reactivity of the clay components in the shale in comparison to tap water, KCl-WBM, and nanosilica.

The nanosilica concentrations did not work as well as the nHAp/SDS concentrations at inhibiting clay from swelling, but they were able to improve the inhibitive capacity of WBM mixed with KCl. Many authors have pointed out that nanosilica particles block the pore throats in shale, which hinders water from entering the shale matrix. This plugging mechanism to a certain degree has hindered the swelling of reactive clay minerals (Luo et al., 2022; Zhong et al., 2020). Moreover, the authors found that, just like most NPs, nanosilica efficiently seals the pores in the shale matrix. The sealing process happens through two different methods: (i) the plugging method, where a single NP of similar size to the pore seals it effectively, and (ii) the bridging method, where several NPs come together to seal a larger pore. However, these studies have also demonstrated that using NPs by themselves effectively seals nanopores but does not fully address microfractures. It can be deduced that utilizing 12 nm-sized nanosilica particles to seal the Endau-Rompin shale pore throat is effective to some extent. This efficiency can be credited to the size of the particles, which matches the diameters of the nanopores.

In addition, Fig. 6b illustrates the effectiveness of nHAp/SDS-injected fluids in preventing clay swelling in KCl-WBM. When nHAp/SDS was added to the shale surfaces, they became hydrophobic (refer to the contact angle data). This implies that water does not adhere to them as much, and clay does not expand or get hydrated (Zhong et al., 2020). This feature will prove advantageous for drilling through shale formations and addressing wellbore instability problems triggered by shale swelling, like borehole collapse. Furthermore, nHAp/SDS particle sizes ranging from 70 to 600 nm appear to be suitable for filling nanopores and microscale pores, cracks, and fractures in shale deposits. A study by Abdullah et al. (2022) shows that most laboratory tests on pore plugging with inhibitors of nanometer size used NPs as powders or suspensions. The average diameter of these NPs was between 5 and 1000 nm, which is the same size range that was used in this study for nHAp/SDS. Zarei and Nasiri (2021) supported the findings of this study in that the size, diameter, concentration, and shape of NPs can affect the inhibitive performance of drilling fluids. The study demonstrates that the nHAp/SDS particles decreased clay swelling and shale-water interaction, enhancing borehole stability by minimizing stresses in the wellbore. The nHAp/SDS particles sealed the pore throats, and formed an internal filter cake, ultimately reducing the fluid flow rate through the shale.

Fig. 6c and d display the findings of the drilling fluids' impact on reducing shale swelling, carried out at a temperature of 80 °C with DLSM. According to the findings, the shale pellets in tap water and KCl-WBM showed an increase in percentage from 19.5 to 33.1 % and 10.1 to 18.8 %, respectively, after 48 h of contact time with a temperature increase from 25 to 80 °C. The KCl-WBM test solution showed around a 43 % reduction in shale swelling when compared to tap water. Fig. 6c illustrates that the concentrations (0.5, 1.0, 1.5, and 2.0 wt%) of nHAp/SDS reduced the swelling of the shale plugs by 29.8–59.6 % compared to the KCl-WBM system. In the same manner, nanosilica concentrations (ranging from 0.5 to 2.0 wt%) decreased the shale plug swelling by 16.5–47.9 % after 48 h of contact time (Fig. 6d). The findings indicated that nHAp/SDS concentrations were more effective than nanosilica concentrations in reducing the swelling percentage of the shale. The nHAp/SDS concentrations decreased the swelling by 60–77 %, while the nanosilica concentrations reduced it by 52.6–70.4 % compared to the reference sample (tap water).

Moreover, the findings clearly show that temperature significantly impacts shale swelling, with higher temperatures leading to increased clay swelling potential (Fig. 6c and d). Overall, the findings indicate that shales exposed to injected fluid at room temperature (25 °C) experience less swelling compared to higher temperatures. The expansion of the shale could be due to water flowing into the shale through chemical osmosis and the activation of clay sites by temperature (Konate and Salehi, 2020). Moreover, it is widely known that as temperature rises, water molecules gain energy and exhibit increased movement within the solution. The molecules find it difficult to line up with the electric field

that results from their interactions with the dissociated ions because of this increased activity (Tian et al., 2021). The shale platelet ions will spread out evenly in solution or in injected fluids because water molecules will surround and dissolve the ions, making the electrostatic forces between them weaker. This leads to the expansion of clay layers and causes the shale to swell (Lalji et al., 2023; Elkatatny, 2018). Furthermore, high temperatures could have caused thermal swelling through the mobilization of clay platelets and their detachment from clay surfaces, leading to higher clay swelling and shale expansion. Fig. 7 illustrates a schematic detailing the process of clay site (platelet) activation through temperature increase.

3.5. Characterization of shale pore structure

Analyzing the shale pore structure involved conducting SEM, contact angle, and ZP tests, as shown in Figs. 8–10. The dried shale specimens of the base mud and 2.0 wt% of nHAp/SDS and nanosilica in linear swell meter tests were examined using SEM to observe the alterations in the microstructure based on compositions (Fig. 8a). When WBM compositions, nanosilica, and nHAp/SDS were mixed in the shale sample, they changed the microstructure. For example, the pores and particle diameters changed, and NP layers formed to act as a barrier. Within the WBM-derived shale specimen, cellulose fibers and bentonite in aggregated form were dispersed and adhered to the surface, entwining between the bentonite particles (Fig. 8a). These loosely connected fiber bundles linked to the clustered particles play a role in increasing the shale's volume, potentially causing decreased permeability (Rana et al., 2020).

Moreover, numerous openings and fissures appeared on the surface of the shale once it had interacted with the base mud (Fig. 8a). Fig. 8b illustrates the development of plugging layers on the shale surface following the application of 2.0 wt% nHAp/SDS. The layers are nicely aligned, particularly from the alkyl and sulphate groups of nHAp/SDS (Fig. 8b). This happened because of the presence of nHAp/SDS, which helps shale platelets settle in a layer-by-layer manner, resulting in the suppression of the shale (Barati et al., 2017). These layers appeared to function as a binder and a barrier, sealing the pores on the surface and preventing water from penetrating the shale due to their hydrophobic nature (Fig. 8b). Moreover, this layer has been demonstrated to decrease shale permeability, control clay swelling, and slow down fluid pressure transmission in shale during the drilling pressure difference (Barati et al., 2017).

Also, as shown in Fig. 8c, blocking layers remained on the surface of the shale after interacting with the base mud containing 2.0 wt% nanosilica. This layer has the ability to inhibit shale swelling and reduce shale permeability. Therefore, nanosilica effectively filled the pore channels of shale that were closest in size or matched its 12 nm size (Zarei and Nasiri, 2021). Nevertheless, there is a possibility that the nanosilica could have aggregated, resulting in the obstruction of the shale's larger pore throats. Based on these findings, it can be deduced that the 12 nm nanosilica blocks the shale's micro- and nano-sized openings and fissures. This illustrates how nanosilica can effectively seal small openings and cracks in shale while drilling. However, the SEM result images indicated that nHAp/SDS has a superior impact.

The water contact angles of shale cores that were submerged in pure nanosilica and nHAp/SDS test fluids are shown in Fig. 9. The shale core sample displayed hydrophilic characteristics, with a water contact angle of 59.1° on the edge of the core sample (Fig. 9a). This behaviour is typical for determining wettability. The water contact angles of pure nanosilica test fluids shown in Fig. 9b–d indicated a high level of hydrophilicity due to their strong attraction to water and ability to adhere to the shale surface. This occurred due to the high surface energy of the 12 nm-sized nanosilica with a surface area of around 175–225 m^2/g (Ngouangna et al., 2022a). Conversely, the nHAp/SDS, functioning as hydrophobic test fluids, caused a sharp increase in the water contact angle on the shale cores' surface. Following the addition of 1.0, 1.5, and 2.0 wt%, the contact angle increased from 59.1° to 127.4°, 128.1°, and 129.4°, respectively (Fig. 9e–g).

It is known that the contact angle serves as an indicator of how wet a solid surface is in a liquid or fluid. According to Yue et al. (2018), the surface tension of the fluid and the characteristics of the surface affect the shape that a drop takes on when it touches a surface. Nevertheless, the contact angles of the nHAp/SDS-injected fluids showed minimal change as the concentration increased, as depicted in Fig. 9e–g. This indicates a limited interaction between the fluids and the shale samples. This phenomenon suggests that the reduced tendency of nHAp/SDS-injected fluids to adhere and absorb onto the shale surface is due to their low wettability or hydrophobic nature. This phenomenon happened due to the low surface tension, resulting in weak adhesion of the nHAp/SDS test fluids to the shale surface. Thus, limited communication between the fluids and the shale samples leads to the observed outcome (Yue et al., 2018).

In addition, the contact angle stays nearly the same as the concentration of nHAp/SDS increases, suggesting that the concentrations have reached their optimal levels. Therefore, any further increase in concentration beyond 0.5 wt% does not seem to have a significant impact on the shale/fluid interface (Ngouangna et al., 2022a). Thus, the nHAp/SDS can modify the shale surface from water-wetting to water-repellent after contact. This is good for reducing clay swelling and retarding clay dispersion and disintegration (Yue et al., 2018). The ability of shale to hydrate and expand is reduced when its surface becomes more hydrophobic (Rana et al., 2020). This outcome validated the LSM and DLSM test analyses and demonstrated that the hydration and swelling of clay minerals could be reduced through wettability alteration.

3.6. ZP magnitude of Endau-Rompin shale

Fig. 10 shows the ZP of the treatment agents (2.0 wt% nanosilica and

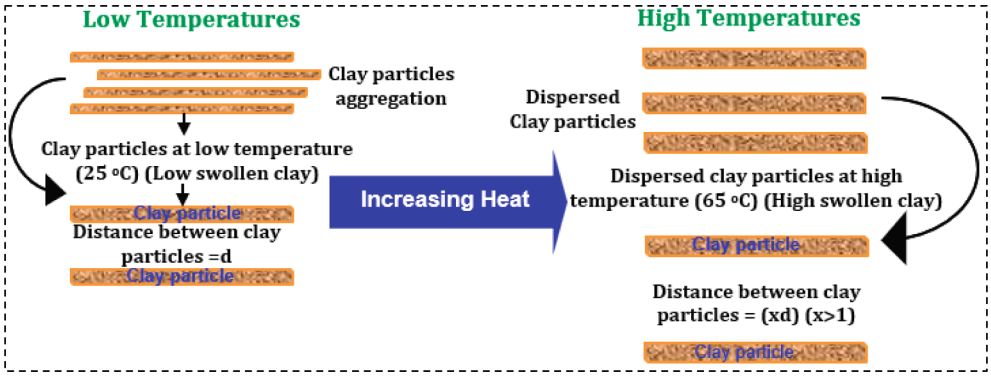

Fig. 7. Clay platelets site activation due to increase in tempperature.

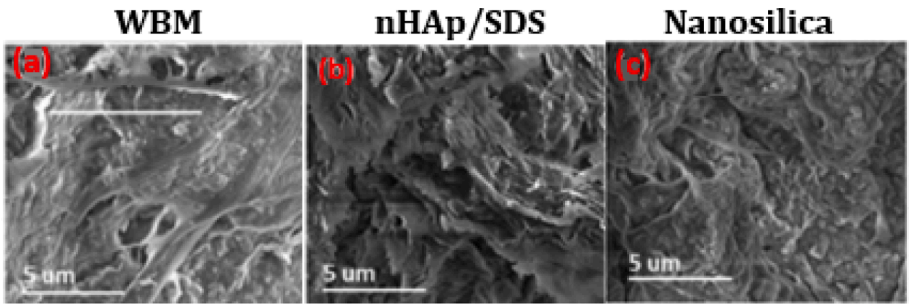

Fig. 8. SEM images of shale specimens in contact with: (a) base mud, (b) 2.0 wt% nHAp/SDS, and (c) 2.0 wt% nanosilica after LSM test at ambient temperature (25 °C).

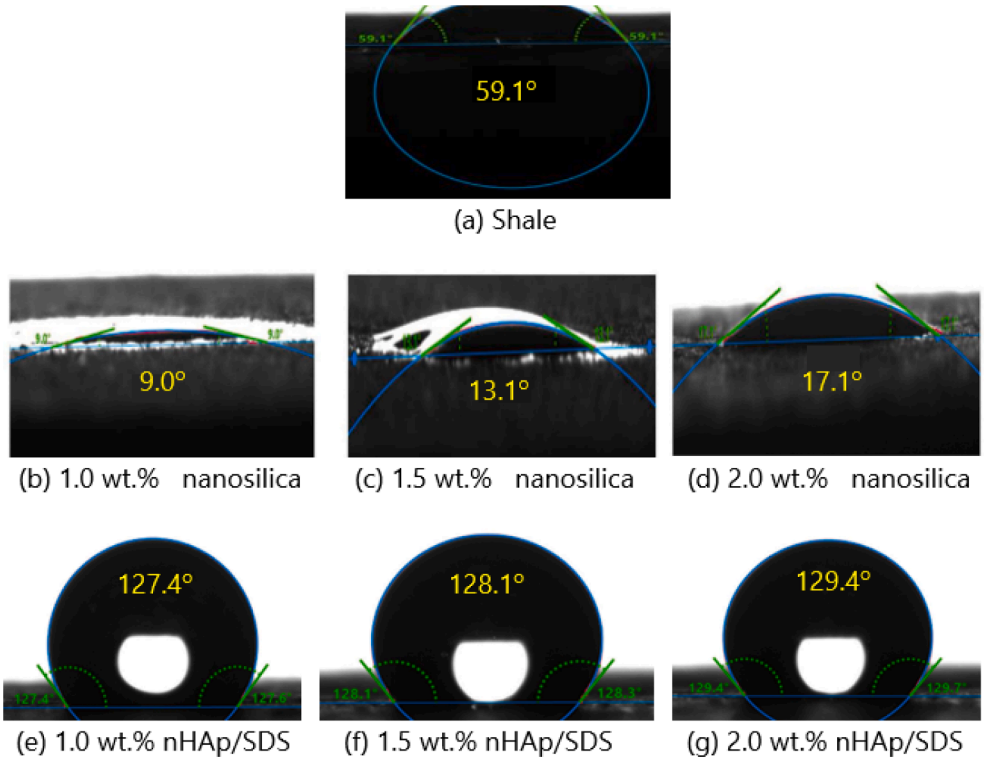

Fig. 9. Water contact angle of (a) shale sample (b-d) nanosilica concentrations, and (e-g) nHAp/SDS concentrations.

2.0 wt% nHAp/SDS) and the Endau-Rompin shale samples that were mixed with the NP test fluids based on their pH levels. As illustrated in Fig. 10, the ZP values of nHAp/SDS and nanosilica test fluids are −42.8 mV and −51.2 mV, respectively, indicating exceptional stability and dispersion. Furthermore, the ZP of the shale sample measured −34.3 mV, indicating a complete dispersion at a pH of 13.2. Upon the addition of nanosilica to the shale dispersion, the ZP of the dispersion experienced a notable shift to –23.7 mV due to the negative charge carried by the nanosilica particles. Regarding nHAp/SDS, there was a notable decrease in the absolute ZP from 34.3 mV to 12.4 mV at a pH of 13.2. Nevertheless, while the nHAp/SDS exhibits a higher absolute ZP compared to the shale sample, the data shown in Fig. 10 demonstrates that nanosilica confers greater stability.

It can also be observed that the ZP of the treatment agents (nanosilica and nHAp/SDS) decreased after being mixed with the shale sample, indicating an interaction between the treatment agents and the shale sample. Regardless of the pH level, both the shale surface and the treatment agents carry negative charges. However, the absolute ZP increases as the pH of the solution increases. With a pH of 13.2, the treatment agents and the shale exhibit a maximum negative charge, suggesting the presence of –OH groups on the surface of nanosilica and SO_4^{2-} groups on the surface of nHAp/SDS (Elochukwu et al., 2017). Likewise, for the shale system, which is also pH-dependent, negative charges were observed, which are responsible for the electrostatic repulsion effect between the treatment agents and the shale. The presence of negative charges leads to a repulsive force between the shale and the treatment agents during face-to-face interaction, ultimately preventing the formation of a connected network structure (Elochukwu et al., 2017). Consequently, the hydration repulsion of the double electrostatic layer was suppressed, resulting in a decrease in the absolute ZP of the shale-nHAp/SDS and shale-nanosilica systems (Zhong et al., 2020).

Nevertheless, as a result of the compression of the hydration repulsion of the double electrostatic layer, the shale particles have a tendency to repel each other, preventing them from aggregating and agglomerating, leading to favourable dispersion in water (Tian et al., 2021; Jiang et al., 2016). The ZP helps in characterizing surface functional groups that affect the wettability of material surfaces. The contact angle results confirm that the treatment agents mixed with shale samples show some level of stability with no obvious signs of agglomeration or flocculation.

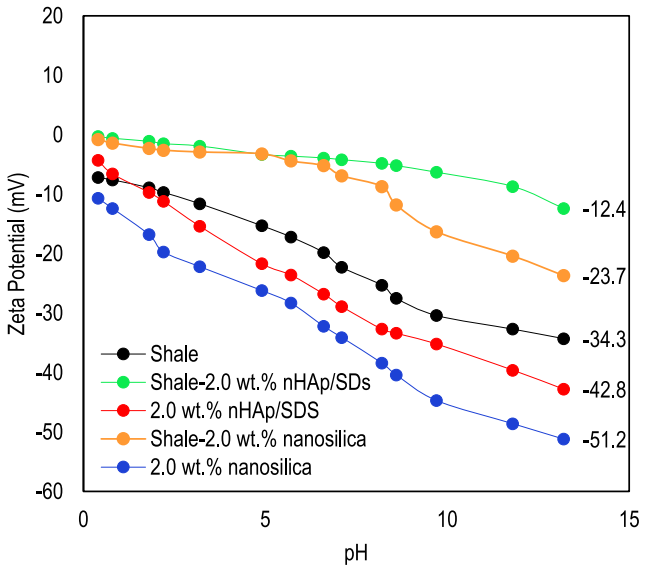

Fig. 10. ZP plots of Endau-Rompin shale samples immersed in 2.0 wt% nanosilica and 2.0 wt% nHAp/SDS after the LSM test at ambient temperature conditions (25 °C).

The findings can be supported by a previous study's report, which emphasized that shale core agglomeration and flocculation primarily happen when the absolute ZP is below 5 mV, approaches zero, and the adsorbed water molecule layer is not present (Tian et al., 2021).

3.7. HTHP suspension stability of nHAp/SDS-based drilling muds

One method to assess the stability of suspensions is by conducting sedimentation tests, which can effectively identify any tendencies towards agglomeration or sedimentation. In this experiment, nHAp/SDS-based drilling muds were aged for 16 h at 120 °C to test their physical stability. They were monitored for 6 days to understand their behaviour against sedimentation, and the results are shown in Fig. 11a and b. The ratio of the sediment height (H_s) to the initial fluid height (H_v) was plotted against time. The stability of the nHAp/SDS fluids can be determined by observing the turbidity and sediment height, which play a significant role in the rheological properties (such as GS and YP) and filtration characteristics (such as FL and FCT) (Moreira et al., 2017). All the liquid samples showed significant settling within the first day (24 h), although some nHAp/SDS samples did not appear to fully settle even after 6 days (144 h). Therefore, the unique settling patterns of various samples were noted within the initial 24 h and assessed based on their tendency to settle.

In comparison with the base mud, the sediment ratios (H_s/H_v) were lower for all nHAp/SDS suspensions within the first 24 h of measurement. The nHAp/SDS fluid suspensions, particularly those with 0.5 and 1.5 wt%, demonstrated excellent sedimentation and colloidal stability over a period of 6 days (144 h). They displayed high turbidity and formed a more compact sediment with a smaller sediment height, in line with the high ZP result shown in Fig. 11. The turbidity of the nHAp/SDS suspension may be closely linked to the hydrophobic alkyl chains of SDS particles dispersed in the fluid system (Daughan et al., 2002). The WBM sedimentation was likely caused by the changing sedimentation rate of PAC-LV fiber-aggregated bentonite, which created turbid colloidal suspensions and sediments phases at the bottom (i.e., solid and suspension phases) (Moreira et al., 2017). The base mud displayed high values of the H_s/H_v ratio, primarily due to the lack of a hydrophobic phase and the effect of high temperature. The nHAp/SDS suspensions showed a gradual settling process with lower ratios than WBM within the first 24 h and even after 144 h (Fig. 11a), suggesting excellent suspension stability.

The impact of ageing time and HTHP on the suspension stability of nHAp/SDS rheological and filtration properties was determined, with the findings presented in Table 5. According to Table 5, the rheological parameters of the base mud were improved with the addition of nHAp/SDS suspensions. The enhancement in the rheological characteristics showed significant improvement with increased concentrations of nHAp/SDS. In comparison to the findings in Table 4 (25 °C), the drilling muds showed varying degrees of suspension stability and thermal stability (Table 5). For example, the viscosity of WBM (25 °C) of 10 cP decreased by 20 % when the temperature was increased from 25 to 120 °C, whereas that of nHAp/SDS suspensions only decreased by 5.3–8.3 % from their initial values at 25 °C. The nHAp/SDS gelation property for cuttings and other weighted materials in the absence of flow during drilling operations exhibited excellent suspension characteristics at high temperatures and after a 6-day ageing period of the fluid samples. In comparison to the reference value of 4.0 lb/100ft^2, the 10-min GS of the base mud rose by 25–75 % between 4.5 and 7 lb/100ft^2 as the nHAp/SDS concentration increased. Furthermore, when the temperature was increased to 120 °C, the 10-min GS did not change, with values at 25 °C varying from 4 to 8 lb/100ft^2 (Table 4).

In addition, the data on filtration properties indicated that the nHAp/SDS suspensions notably reduced the HTHP FL of the base mud to a range of 9.1 to 4.8 mL, representing a decrease of 38–70 % from the reference value of 14.6 mL. The increased fluid loss of the base mud demonstrates the impact of the high sedimentation ratio linked to the mud, resulting in a thick filter cake compared to the nHAp/SDS test fluids. This finding suggests that the high temperature does not have a notable impact on the suspension characteristics of nHAp/SDS test

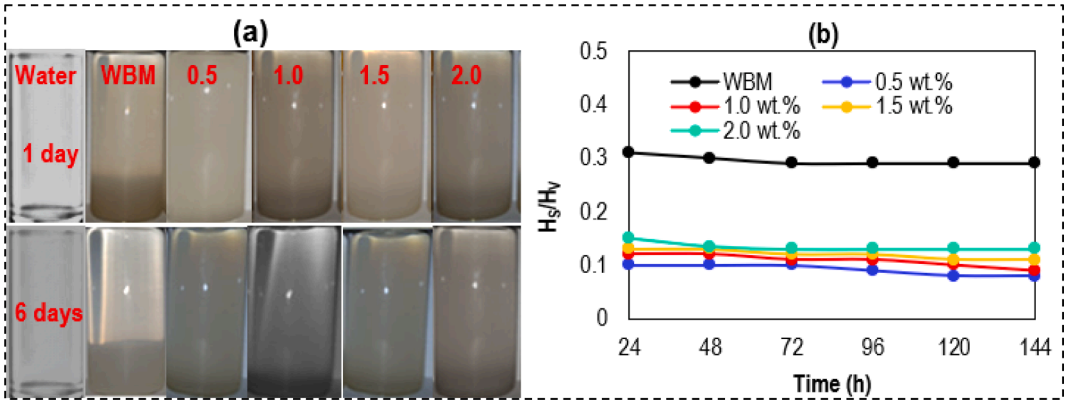

Fig. 11. Illustration of the dispersion levels of nHAp/SDS suspensions for 144 h (6 days): (a) Captured digital images of fluid suspensions and (b) ratio of the height of sediment (H_s) to the initial fluid height (H_v) versus time after aging for 16 h at 120 °C in a roller oven (the drilling fluids used are based on the recipe in Section 2.6).

Table 5
HTHP filtration and rheological properties of nHAp/SDS-based fluid suspensions after hot-rolling for 16 h at 120 °C (aged for 6 days) using the mud formulation in Section 2.6.

Base mud	nHAp/SDS	θ_{600}	θ_{300}	GS 10 s (lb/100ft^2)	GS 10 min (lb/100ft^2)	PV (cP)	AV (cP)	YP (lb/100ft^2)	FL (mL)	FCT (mm)
WBM	0.0 wt%	25	17	3.0	4.0	8	12.5	9	14.6	2.28
WBM	0.5 wt%	32	21	3.0	4.0	11	16	10	9.1	0.92
WBM	1.0 wt%	38	24	3.5	5.0	14	19	10	7.7	0.89
WBM	1.5 wt%	42	27	4.0	6.0	15	21	12	6.3	0.78
WBM	2.0 wt%	50	32	5.0	7.0	18	25	14	4.4	0.56

fluids. Nevertheless, it diminishes the fluid properties of the base mud and increases its sedimentation ratio. This occurrence is a result of the reduction in cohesive forces among the fluid molecules, leading to an increase in energy within the materials due to molecular vibrations (Elkatatny, 2018).

3.8. Compatibility findings of nHAp/SDS

According to the data displayed in Fig. 12, the addition of 2.0 wt% of nHAp/SDS does not have any negative impact on the rheological and filtration characteristics of both the WBDF and the HPDF. The conclusion that can be drawn from this is that nHAp/SDS is completely compatible with other additives for drilling muds that are often used in the oil and gas industry. Furthermore, the fluid loss of the nHAp/SDS are smaller than those of the drilling muds without nHAp/SDS.

4. Shale stabilization mechanisms

4.1. Nanosilica as a shale plugging agent

Physical plugging is proposed as the mechanism through which nanosilica inhibits swelling and dispersion of shale samples, based on this study. Shale formations have many nano- and microscale fractures, fissures, and pores. Abdullah et al. (2022) explained that clay particles with a strong affinity for water may infiltrate shale pores and fissures during drilling, leading to borehole instability. Nanosilica inhibits clay swelling and hydration by physically blocking nanopore throats and microcracks, reducing shale permeability (Saleh et al., 2021). This mechanism was supported by Li et al. (2022), Luo et al. (2022), Abdullah et al. (2022), Zarei and Nasiri (2021), and Zhong et al. (2020). The authors discovered that nanosilica particles are trapped in the nano- and micropores of shale reservoirs. This hinders the interaction between shale and water, lowers the permeability of shale, and inhibits clay from swelling. Abdullah et al. (2022) identified two criteria necessary for nanosilica to plug shale pores. (1) Owing to its comparable size to nanopores, a single nanosilica particle may easily enter shale pores and become trapped. Nanosilica seals the shale nanopores, preventing fluid or water from entering the shale sample due to its very low permeability. The nanosilica used in this study has a diameter of 12 nm, which is the same size as shale nanopores, which are between 10 and 30 nm (Abdullah et al., 2022). (2). The bridging process takes place when many nanosilica particles plug micro-shale pores that are bigger than a single nanosilica particle (Huang et al., 2018). LSM, DLSM, and hot-rolling dispersion recovery support the pore plugging process, which decreases clay swelling and hydration.

4.2. The mechanism of shale stabilization by nHAp/SDS

Fig. 13 illustrates the inhibitory effect of nHAp/SDS on clay swelling. The shale sample mostly interacts with nHAp/SDS particles by physisorption and physical plugging. According to Rana et al. (2020), the electrostatic interaction between negatively charged SDS particles and positively charged clay particles is what causes the process of physisorption. These induce the attachment of nHAp and SDS particles to the shale surface. When water and clay interact, the negatively charged aluminosilicate layers in the clay attract and bond with the positively charged Na^+. This results in the shale expanding. The contact angle results show that intercalating ions like Na^+, Ca^{2+}, and Mg^{3+} make clay surfaces more water-friendly (Muhammed et al., 2021). Clay surfaces expand due to electrostatic attraction and osmotic pressure, allowing water to enter porous clay formations. nHAp/SDS particles interact with the shale (Fig. 13) to prevent clay swelling. SDS's negatively charged SO_4^{2-} (hydrophilic head group) interacts with the oppositely charged edges of the clay through its hydrophilic component (Muhammed et al., 2021).

The contact angle findings (Fig. 13) show that the SDS alkyl chain (hydrophobic part) makes the surface of the shale less permeable to water (Koroleva et al., 2020; Li and Ishiguro, 2016). This impedes water

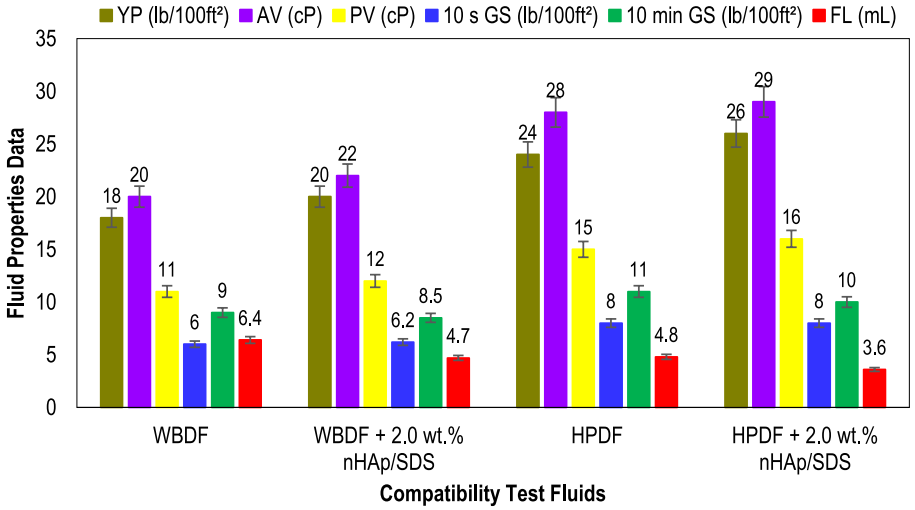

Fig. 12. Illustration of nHAp/SDS compatibility on the rheological and filtration properties of WBDF and HPDF (test fluid recipes can be found in Section 2.7).

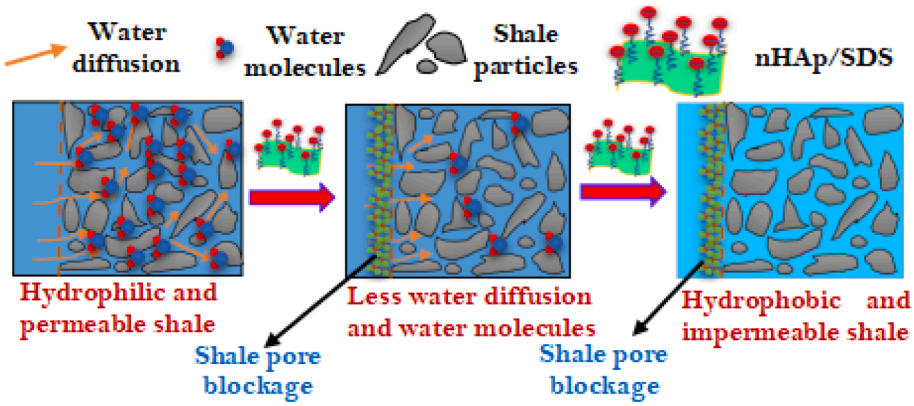

Fig. 13. Mechanism of shale stabilization by nHAp/SDS particles.

infiltrating the shale. The hydrophobic part forms a colloidal layer on the surface of the shale and the wall of the wellbore. This layer hinders filtrate from penetrating and water from entering the shale (Abdullah et al., 2022). Along with the physisorption process, the nHAp/SDS particles (70–600 nm) plugged the cracks and pores in the shale and prevented water from penetrating it. This eliminates the chance of clay particle osmotic swelling (Muhammed et al., 2021). The collective mechanism's description of nHAp/SDS conforms with the results obtained from SEM, LSM, DLSM, ZP, contact angle, filtration, and rheological parameters.

5. Conclusions

This study used the chemical precipitation approach to synthesize nHAp/SDS particles in situ, which functioned as shale inhibitors in WBM. Rheological and filtration property measurements showed the effects of nHAp/SDS on the properties of WBM. Additionally, using DLSM and LSM tests, the inhibitive and shale stability performances of nHAp/SDS, nanosilica, and KCl-WBM in Endau-Rompin shale dominated by smectite-clays were assessed. More tests were conducted to further comprehend the inhibitory performance of nHAp/SDS. These include contact angle, ZP, SEM, stability, compatibility, and hot-rolling dispersion tests. The following are some of the most important conclusions drawn from this study:

1. At 25 °C, nHAp/SDS and nanosilica concentrations resulted in a noticeable increase in plastic viscosity of 20–90 % and 10–70 %, respectively, compared to the KCl-WBM system at 10 cP. In the same manner, the fluid loss was notably reduced by a range of 19–61 % with nHAp/SDS concentrations and 8–42 % with nanosilica concentrations compared to the reference sample (KCl-WBM) of 7.9 mL.
2. With the addition of 2.0 wt% nHAp/SDS to KCl-based WBM, the shale swelling using LSM at 25 °C decreased from 10.1 % to 4.7 % (by 53.4 %). This outperformed nanosilica, which decreased the shale swelling from 10.1 % to 6.1 % (a reduction of 39.6 %).
3. With the increase in the amount of nHAp/SDS and nanosilica in the base fluid, the retarding of shale from dispersion improved, leading to an increase in the shale rolling recovery rate. Between 65 and 120 °C, the recovery rate of hot-rolled shale plugs with KCl-WBM increased from 89.8 to 96.2 % and 76.6 to 88.8 %, from the initial rates of 52.1–63.3 % using nHAp/SDS and nanosilica, respectively.
4. Increased temperatures enhance the clay's tendency to swell because of the increased activation of the clay platelets. Between 25 and 80 °C, DLSM test revealed that the shale plug height expand from 6.1 to 9.8 % for 2.0 wt% nanosilica, 4.7–7.6 % for 2.0 wt% nHAp/SDS, and 10.1–18.8 % for KCl-WBM.
5. The study findings indicated that the nHAp/SDS test fluids are in harmony with WBDF and HPDF. Furthermore, they maintain a stable suspension even after being aged for 6 days, providing an advantageous characteristic of the long-term stability of drilling fluids.
6. Based on the contact angle test results, it is evident that nHAp/SDS exhibits hydrophobic characteristics, leading to a decrease in shale-water interaction. The fluid properties of nHAp/SDS outperformed those of nanosilica under all drilling conditions.
7. Altogether, the study found that nHAp/SDS particles in WBM can contribute to promoting wellbore stability and increasing the performance of drilling fluids. Furthermore, this study and various research on nano-scale particles (5 nm–1000 nm) have brought attention to important findings, constraints, and potential opportunities for future research.

6. Significance, limitations, and future opportunities

The ability of nHAp/SDS to prevent clay swelling and hinder shale dispersion can improve wellbore stability. KCl and nHAp/SDS work together to prevent clay swelling and slow down shale dispersion, resulting in favourable WBM characteristics. Still, nHAp/SDS could not completely form an impermeable filter cake and hydrophobic surface to inhibit shale swelling due to its size not perfectly aligning with the 10–30 nm nanopores of shale (Abdullah et al., 2022). Therefore, the NP type and concentration should be sufficient for shale coverage and stabilization. In the Endau-Rompin shale, nanosilica particles measuring 12 nm are found to partially obstruct the pore throats of the shale. Particles ranging from 70 to 600 nm of nHAp/SDS showed superior performance. With higher amounts of nanosilica and nHAp/SDS, the inhibition performance improved.

Various studies (Luo et al., 2022; Muhammed et al., 2021; Abdullah et al., 2022; Rana et al., 20120; Hoxha et al., 2019; Wang et al., 2018; Aftab et al., 2016; Mao et al., 2015), have shown that an excessive amount of NPs or microparticles in a fluid system can lead to challenges in cost and effectiveness. Hence, utilizing hydrophobic nanosized materials at optimal concentrations may prove to be a more practical and efficient approach for shale stabilization. The identified limitations highlight intriguing challenges and potential opportunities for deploying nanosized diameter-based drilling fluids in the field to maintain borehole stability. The effectiveness of the borehole may vary based on:

1. The specific kind of nano-range-diameter particles and ZP of the drilling fluid;
2. Specific shale kind, especially ZP of the drilling fluid;
3. The interaction between drilling fluid containing specific nano-range-diameter particles and shale
4. The nano-range diameters' ionic strength, hydrophilicity, or hydrophobicity, shape, and average diameter relative to the shale's average pore throat size;

5. The nano-range diameter concentration needed to cover the shale surface
6. Finally, temperature, pressure, salt type and concentration, and fluid pH in the downhole environment where nano-range-diameter fluids are administered affect them.

These variables should guide the design of high-performance WBM, which is now on the priority lists of drilling fluid service firms and oil company operators owing to OBM constraints. Future applications of nano-range diameters may help maximize the production of potentially accessible hydrocarbons via drilling or improved oil recovery. However, cutting-edge research, appropriate drilling practices, and technological integration of drilling fluids and NPs, or nano-microparticles, are needed to access producible hydrocarbons within complicated reservoirs and geological formations.

Declaration of competing interest

The authors declare that they have no known competing financial interests or personal relationships that could have appeared to influence the work reported in this paper.

Acknowledgement of funding source

The authors would like to acknowledge the financial support from the Ministry of Higher Education (MOHE), Malaysia, under the Fundamental Research Grant Scheme (FRGS) via reference number FRGS/PV/2022/03075 and Universiti Teknologi Malaysia for the funding under UTM Fundamental Research (UTMFR) (Q.J130000.21A2.06E09) and the Fundamental Research Grant Scheme (FRGS) (Ref: FRGS/1/2023/TK09/UTM/02/13). Engr. Dr. Jeffrey Onuoma Oseh is a researcher at UTM under the postdoctoral fellowship scheme for the project "Evaluation of Modified Hydroxyapatite Nanoparticles for Rheological and Filtration Properties Modification in Field-Applicable Drilling Muds".

References

Abatan, A.O., Akinyemi, O.D., Olowofela, J.A., G.A., Ajiboye, F.K., Salako., 2016. Experimental investigation of factors affecting compressional and shear wave velocities in shale and limestone of Ewekoro formation of Southern Nigeria sedimentary basin. Environ Earth Sci, 75, 1442. doi: 10.1007/s12665-016-6229-6.

Abdullah, A.Z., Ridha, S., Mohshim, D.F., Yusuf, M., Kamyab, H., Krishna, S., Maoinser, M.A., 2022. A comprehensive review of nanoparticles: Effect on water-based drilling fluids and wellbore stability, Chemosphere, 308. Part 1, 136274.

Abidi, S.S.A., Murtaza, Q., 2014. Synthesis and characterization of nano-hydroxyapatite powder using wet chemical precipitation reaction. J. Mater. Sci. Technol. 30 (4), 307–310.

AL-Bazali, T., 2021. Insight on the inhibitive property of potassium ion on the stability of shale: a diffuse double-layer thickness (k−1) perspective. J. Pet. Explor. Prod. Technol. 11, 2709–2723.

An, Y., Yu, P., 2018. A strong inhibition of polyethyleneimine as shale inhibitor in drilling fluid. J. Pet. Sci. Eng. 161, 1–8.

API recommended practice 13B-2., 2019 In: API Standard Practice for Field Formulation Water–Based Drilling Fluids, fifth ed.

Bai, X., Wang, H., Luo, Y., Zheng, X., Zhang, X., Zhou, S., Pu, X., 2017. The structure and application of amine terminated hyperbranched polymer shale inhibitor for water-based drilling fluid. J. Appl. Polym. Sci. 134 (46), 454466.

Barati, P., Shahbazi, K., Kamari, M., Aghajafari, A., 2017. Shale hydration inhibition characteristics and mechanism of a new amine-based additive in water-based drilling fluids. Petroleum 3 (4), 476–482. https://doi.org/10.1016/j.petlm.2017.05.003.

Blkoor, S.O., Norddin, M.N.A.B.M., Ismail, I., Oseh, J.O., Saeed, S.S., Risal, A.A., Sariman, M.F., Ngouangna, E.N., 2023. Enhancing the stability of shale in water-based fluid with polyethylene glycol/nanosilica composite grafted with sodium dodecyl sulfate. Arab J Geosci 16, 541. https://doi.org/10.1007/s12517-023-11653-1.

Bulina, N.V., Makarova, S.V., Baev, S.G., Matvienko, A.A., Gerasimov, K.B., Logutenko, O.A., Bystrov, V.S., 2021. A Study of Thermal Stability of Hydroxyapatite. Minerals 11, 1310. https://doi.org/10.3390/min11121310.

Córdova-Udaeta, M., Kim, Y., Yasukawa, K., Kato, Y., Fujita, T., Dodbiba, G., 2021. Study on the Synthesis of Hydroxyapatite under highly Alkaline Conditions. Ind. Eng. Chem. Res. 60, 4385–4396.

Daugan, S., Talini, L., Herzhaft, T., Allain, C., 2002. Aggregation of particles settling in shear-thinning fluids. Part 1. Two-Particle Aggregation. Eur. Phys. J. E 7, 73–81.

Elkatatny, S., 2018. Enhancing the Stability of Invert Emulsion Drilling Fluid for Drilling in High-Pressure High-Temperature Conditions. Energies 11, 2393. https://doi.org/10.3390/en11092393.

Elochukwu, H., Gholami, R., Dol, S.S., 2017. An approach to improve the cuttings carrying capacity of nano silica-based muds. J Pet Sci Eng. 152, 210–216.

Ferreira, C.C., Teixeira, G.T., Lachter, E.R., Nascimento, R.S.V., 2016. Partially hydrophobized hyperbranched polyglycerols as non-ionic reactive shale inhibitors for water-based drilling fluids. Appl. Clay Sci. 122–123, 122–132.

Hale, A.H., Mody, F.K., 1993. Partially hydrolyzed polyacrylamide (PHPA) mud systems for Gulf of Mexico deep-water prospects. Paper presented at the SPE International Symposium on Oilfield Chemistry, New Orleans, Louisiana.

He, S., Liang, L., Zeng, Y., Ding, Y., Lin, Y., Liu, X., 2016. The influence of water-based drilling fluid on mechanical property of shale and the wellbore stability. Petroleum 2, 61–66. https://doi.org/10.1016/j.petlm.2015.12.002.

Hoxha, B.B., Sullivan, G., van Oort, E., Daigle, H., Schindler, C., 2016. Determining the Zeta Potential of Intact Shales via Electrophoresis. Society of Petroleum Engineers. https://doi.org/10.2118/180097-MS.

Huang, X., Shen, H., Sun, J., Lv, K., Liu, J., Dong, X., Luo, S., 2018. Nanoscale laponite as a potential shale inhibitor in water-based drilling fluid for stabilization of wellbore stability and mechanism study. ACS Appl. Mater. Interfaces 10, 33252–33259.

Huang, D., Xie, G., Hu, P., Hu, S., Zhao, Z., Li, W., Deng, M., Luo, P., 2020. Improved analysis methods to study the behavior of potassium ions in the interlayer of montmorillonite. J. Mater. Res. Technol. 9 (4), 7754–7761.

Jamarun, N., Trycahyani1, N.A., Arief, S., Septiani, U., Sisca, V., 2023. Synthesis of Hydroxyapatite-Polyethylene Glycol with In-Situ Method Using Calcium Oxide from Blood Shells (Anadara granosa). Indones. J. Chem. 23 (3), 618–626.

Jia, H., Huang, P., Han, Y., Wang, Q., Jia, K., Sun, T., Zhang, F., Yan, H., Lv, K., 2019. Investigation for the novel use of a typical deep eutectic solvent as a potential shale inhibitor. Energy Sources Part A 1–14. https://doi.org/10.1080/15567036.2019.1643953.

Jiang, T., Jin, Z., Liu, G., Hu, Z., Chen, X., Liu, Z., Wang, G., 2022. Investigating the Pore Structure Characteristics and Reservoir Capacities of Lower Jurassic Continental Shale Reservoirs in the Northeastern Sichuan Basin. China. Front. Earth Sci. 10, 886907.

Jiang, G., Qi, Y., An, Y., Huang, X., Ren, Y., 2016. Polyethyleneimine as shale inhibitor in drilling fluid. Appl. Clay Sci. 127–128, 70–77.

Konate, N., Salehi, S., 2020. Experimental Investigation of Inhibitive Drilling Fluids Performance: Case Studies from United States Shale Basins. Energies 2020 (13), 5142.

Koroleva, M.Y., Karakatenko, E.Y., Yurtov, E.V., 2020. Synthesis of hydroxyapatite nanoparticles by controlled precipitation in the presence of sodium dodecyl sulfate. Colloid J. 82 (3), 275–283.

Lalji, S.M., Khan, M.A., Haneef Ali, S.I., Arain, A.H., Shah, S.S., 2023. Nano-particles adapted drilling fluids for the swelling inhibition for the Northern region clay formation of Pakistan. Appl Nanosci 13, 503–517. https://doi.org/10.1007/s13204-021-01825-4.

Li, P., Ishiguro, M., 2016. Adsorption of anionic surfactant (sodium dodecyl sulfate) on silica. Soil Sci. Plant Nutr. 62 (3), 223–229.

Li, X., Jiang, G., Yang, L., Wang, K., Shi, H., Li, G., Wu, X., 2019. Application of Gelatin Quaternary Ammonium Salt as an Environmentally Friendly Shale Inhibitor for Water-Based Drilling Fluids. Energy Fuel 33 (9), 9342–9350.

Luo, X., Jiang, G., Wang, G., Yang, L., He, Y., Cui, K., Yang, J., 2022. Novel approach to improve shale stability using super-amphiphobic nanoscale materials in water-based drilling fluids and its field application. Reviews on Adv. Mat. Sci. 61 (1), 41–54.

Manafi, S.A., Yazdani, B., Rahimiopour, M.R., Sadrnezhaad, S.K., Amin, M.H., Razavi, M., 2008. Synthesis of nano-hydroxyapatite under a sonochemical/hydrothermal condition. Biomed. Mater. 3 (2), 025002 https://doi.org/10.1088/1748-6041/3/2/025002.

Mao, H., Qiu, Z., Shen, Z., Huang, W., 2015. Hydrophobic associated polymer-based silica nanoparticles composite with core–shell structure as a filtrate reducer for drilling fluid at ultra-high temperature. J. Petrol. Sci. Eng. 129, 1–15.

Moreira, B.A., Arouca, F.O., Damasceno, J.J.R., 2017. Analysis of suspension sedimentation in fluids with rheological shear-thinning properties and thixotropic effects. Powder Technol. 308, 290–297.

Moukoko, A.D.K., Yang, L., Jiang, G., Chang, X., Dong, T., 2023. Effect of Alkylation Chain Length on Inhibiting Performance of Soluble Ionic Liquids in Water-Based Drilling Fluids. ACS Omega 8 (6), 5939–5946. https://doi.org/10.1021/acsomega.2c07796.

Muhammed, N.S., Olayiwola, T., Elkatatny, S., Haq, B., Patil, S., 2021. Insights into the application of surfactants and nanomaterials as shale inhibitors for water-based drilling fluid: A review. J. Nat. Gas Sci. Eng. 92, 103987.

Naeimavi, M., Khazali, F., Abdideh, M., Saadati, Z., 2020. Interference of Sodium Chloride on Shale Stabilization with Potassium Chloride in Drilling Fluid. J. Pet. Sci. Technol. 10 (1), 30–36. https://doi.org/10.22078/jpst.2020.3885.1616.

Ngouangna, E.N., Jaafar, M.Z., Norddin, M.N.A.M., Agi, A., Oseh, J.O., Mamah, S., 2022a. Surface Modification of Nanoparticles to Improve Oil Recovery Mechanisms: A Critical Review of the Methods, Influencing Parameters, Advances and Prospects. J. Mol. Liq. 360.

Ngouangna, E.N., Jaafar, M.Z., Norddin, M.N.A.M., Agi, A., Risal, A.R., Mamah, S.C., Oseh, J.O., 2022b. The Effect of Hydroxyapatite Nanoparticles on Wettability and Brine-Oil Interfacial Tension as Enhance Oil Recovery Mechanisms. J. Pet. Sci. Eng. 218.

Oseh, J.O., Norddin, M.N.A.M., Ismail, I., Gbadamosi, A.O., Agi, A., Mohammed, H.N., 2019. A novel approach to enhance rheological and filtration properties of water–based mud using polypropylene–silica nanocomposite. J. Pet. Sci. Eng. 181, 106264.

Oseh, J.O., Mohd Norddin, M.N.A., Ismail, I., Ismail, A.R., Gbadamosi, A.O., Agi, A., Ogiriki, S.O., 2020a. Investigating almond seed oil as potential biodiesel-based drilling mud. In: Journal of Petroleum Science and Engineering, pp. 1–15.

Oseh, J.O., Norddin, M.N.A.M., Mohammed, H.N., Ismail, I., Gbadamosi, A.O., Agi, A., Ismail, A.R., Blkoor, S.O., 2020b. Influence of (3–Aminopropyl) triethoxysilane on entrapped polypropylene at nanosilica composite for shale swelling and hydration inhibition. J. Pet. Sci. Eng. 194, 107560.

Oseh, J.O., Mohd Norddin, M.N.A., Gbadamosi, A.O., Agi, A., Blkoor, S.O., Ismail, I., Igwilo, K.C., Igbafe, A.I., 2023a. Polymer nanocomposites application in drilling fluids: A review. Geoenergy Science and Engineering. 222.

Oseh, J.O., Norddin, M.N.A.M., Ismail, I., Duru, U.I., Gbadamosi, A.O., Agi, A., Ngouangna, E.N., Blkoor, S.O., Yahya, M.N., Risal, A.R., 2023b. Rheological and filtration control performance of water-based drilling muds at different temperatures and salt contaminants using surfactant-assisted novel nanohydroxyapatite. In: Geoenergy Science and Engineering, pp. 1–18.

Prakash, V.C.A., Venda, I., Thamizharasi, V., Sathya, E., 2021. A new attempt on synthesis of spherical nano hydroxyapatite powders prepared by dimethyl sulfoxide – poly vinyl alcohol assisted microemulsion method. Mater. Chem. Phys. 259, 124097.

Prasad, P.S., Marupalli, B.C.G., Das, S., Das, K., 2023. Surfactant-assisted synthesis of hydroxyapatite particles: a comprehensive review. J Mater Sci 58, 6076–6105.

Qiao, B., Liang, Y., Wang, T.J., Jiang, Y., 2016. Surface modification to produce hydrophobic nano-silica particles using sodium dodecyl sulfate as a modifier. Appl. Surf. Sci. 364, 103–109. https://doi.org/10.1016/j.apsusc.2015.12.116.

Rahman, M.T., Negash, B.M., Danso, D.K., Idris, A., Elryes, A.A., Umar, I.A., 2021. Effects of imidazolium- and ammonium-based ionic liquids on clay swelling: experimental and simulation approach. J. Pet. Explor. Prod. Tech. 12 (5).

Saleh, T.A., Rana, A., Arfaj, M.K., Ibrahim, M.A., 2021. Hydrophobic polymer-modified nanosilica as effective shale inhibitor for water-based drilling mud. J. Pet. Sci. Eng. 209, 109868.

Sehly, K., Chiew, H.L., Li, H., Song, A., Leong, Y.K., Huang, W., 2015. Stability and ageing behaviour and the formulation of potassium-based drilling muds. Appl. Clay Sci. 104, 309–317. https://doi.org/10.1016/j.clay.2014.12.013.

Sharma, R., Patel, K.S., Lata, L., Milosh, H., 2016. Characterization of Urban Soil with SEM-EDX. Am. J. Anal. Chem. 07, 724–735. https://doi.org/10.4236/ajac.2016.

Shi, Z., Huang, X., Cai, Y., Tang, R., Yang, D., 2009. Size effect of hydroxyapatite nanoparticles on proliferation and apoptosis of osteoblast-like cells. Acta Biomater. 5 (1), 38–45.

Sudharsan, J., Khare, S.K., 2023. Pore pressure transmission test as measure of shale inhibition performance of nanoparticle additives in water-based drilling fluids – A comprehensive review. Mater. Today:. Proc. https://doi.org/10.1016/j.matpr.2023.04.148.

Tian, Y., Liu, X., Luo, P., Huang, J., Xiong, J., Liang, L., Li, W., 2021. Study of a Polyamine Inhibitor Used for Shale Water-Based Drilling Fluid. ACS Omega 6 (23), 15448–15459.

Villada, Y., Gallardo, F., Erdmann, E., Casis, N., Olivares, L., Estenoz, D., 2017. Functional characterization on colloidal suspensions containing xanthan gum (XGD) and polyanionic cellulose (PAC) used in drilling fluids for a shale formation. Appl. Clay Sci. 149, 59–66.

Xie, G., Xiao, Y., Bai, Y., Luo, Y., Wang, R., Gu, S., 2022. Synthesis of alkyl polyamine with different functional groups and its montmorillonite swelling inhibition mechanism: Experiment and density functional theory simulation. Appl. Clay Sci. 230, 106715.

Xu, J., Qiu, Z., Huang, W., Zhao, X., 2017. Preparation and performance properties of polymer latex SDNL in water-based drilling fluids for drilling troublesome shale formations. J. Nat. Gas Sci. Eng. 37, 462–470.

Yang, X., Cai, J., Jiang, G., Chen, S., Yue, Y., Shi, Y., Wei, Z., 2021. A method of determining osmotic pressure for low-clay shale with different salt ions considering effect of dynamic permeability on flow. Eng. Geol. 295, 106434.

Yang, L., Jiang, J., Shi, Y., Yang, X., 2017. Application of Ionic Liquid and Polymeric Ionic Liquid as Shale Hydration Inhibitors. Energy Fuel 31 (4), 4308–4317.

Yang, Y., Yang, X., Wang, T., Jiang, G., Luckham, P.F., Li, X., Shi, H., Luo, J., 2019. Effect of alkyl chain length on shale hydration inhibitive performance of vinylimidazolium-based ionic liquids Ind. Eng. Chem. Res. 58, 8565–8577.

Yue, Y., Chen, S., Wang, Z., Yang, X., Peng, Y., Cai, J., Nasr-El-Din, H.A., 2018. Improving wellbore stability of shale by adjusting its wettability. J. Pet. Sci. Eng. 161, 692–702.

Zaitoun, A., Berton, N., 1996. Stabilization of montmorillonite clay in porous media by polyacrylamides. In: SPE Formation Damage Control Symposium. SPE.

Zarei, V., Nasiri, A., 2021. Stabilizing Asmari Formation interlayer shales using water-based mud containing biogenic silica oxide nanoparticles synthesized. J. Nat. Gas Sci. Eng. 91, 103928 https://doi.org/10.1016/j.jngse.2021.103928.

Zhang, C., Pathegama Gamage, R., Perera, M.S.A., Zhao, J., 2017. Characteristics of Clay-Abundant Shale Formations: Use of CO_2 for Production Enhancement. Energies 10, 1887. https://doi.org/10.3390/en10111887.

Zhang, F., Sun, J., Dai, Z., Chang, X., Huang, X., Liu, J., Wang, Z., Lv, K., 2020. Organosilicate polymer as high temperature Resistant inhibitor for water-based drilling fluids. J. Polym. Res. 641, 128489.

Zhong, H., Qiu, Z., Huang, W., Cao, J., 2012. Poly (oxypropylene)-amidoamine modified bentonite as potential shale inhibitor in water-based drilling fluids. Appl. Clay Sci. 67, 36–43. https://doi.org/10.1016/j.clay.2012.06.002.

Zhong, H., Gao, X., Zhang, X., Qiu, Z., Zhao, C., Zhang, X., Jin, J., 2020. Improving the shale stability with nano-silica grafted with hyperbranched polyethyleneimine in water-based drilling fluid. J. Nat. Gas Sci. Eng. 83, 103624.